Hindawi Publishing Corporation
International Journal of Photoenergy
Volume 2009, Article ID 294042, 22 pages
doi:10.1155/2009/294042

*Review Article*

# Doping of $TiO_2$ Polymorphs for Altered Optical and Photocatalytic Properties

**Xiliang Nie,[1,2] Shuping Zhuo,[1,3] Gloria Maeng,[1] and Karl Sohlberg[1]**

[1] *Department of Chemistry, Drexel University, 3141 Chestnut Street, Philadelphia, PA 19104, USA*
[2] *Hampton University Proton Therapy Institute, Hampton, VA, USA*
[3] *School of Chemical Engineering, Shandong University of Technology, Zibo 255049, China*

Correspondence should be addressed to Karl Sohlberg, kws24@drexel.edu

Received 25 March 2009; Revised 17 July 2009; Accepted 13 September 2009

Recommended by Franca Morazzoni

This paper reviews recent investigations of the influence of dopants on the optical properties of $TiO_2$ polymorphs. The common undoped polymorphs of $TiO_2$ are discussed and compared. The results of recent doping efforts are tabulated, and discussed in the context of doping by elements of the same chemical group. Dopant effects on the band gap and photocatalytic activity are interpreted with reference to a simple qualitative picture of the $TiO_2$ electronic structure, which is supported with first-principles calculations.



## 1. Introduction

$TiO_2$ is the prototypical photocatalyst for water dissociation [1–4], and the most common paint opacifying agent [5], but is not ideal for either application. Both applications are dependant upon its optical properties. Unfortunately for photocatalysis, $TiO_2$ has a band-gap of ca 3.0 eV. This means that deep violet or ultraviolet photons are required to populate the conduction band (which endows the material with sufficient reducing power to reduce water) but the bulk of solar radiation that reaches the Earth's surface is in the 1.0–1.9 eV range. By contrast, for application as a paint opacifier, it would be desirable to *decrease* the photocatalytic efficiency of $TiO_2$ since it catalyzes the formation of radicals which in turn lead to degradation of the organic binders in paint. In short, there is great interest in tuning the optical properties of $TiO_2$.

In the past half decade there have been numerous attempts at modifying the band gap (bg) of $TiO_2$ by doping. Early success in reducing the band gap was achieved with nitrogen doping of the anatase-phase [6]. Shortly thereafter, carbon doping of a predominantly rutile phase $TiO_2$ film was shown to produce even more promising results [7], decreasing the band gap while producing a material with photoconversion efficiency comparable to that of undoped n-type $TiO_2$. It was demonstrated that when carbon is substituted for some of the lattice oxygen so that the stoichiometry may be written $TiO_{2-x}C_x$, ($x \approx 0.15$) there is appreciable optical absorption at wavelengths shorter than 535 nm (2.32 eV). Remarkably, such carbon doping produces a "double band gap" feature; whereby there are two marked onsets in the optical absorption spectrum, one at the above-mentioned 535 nm and another at 440 nm.

Contemporaneously, numerous experimental and theoretical studies were carried out in an effort to better understand $TiO_2$ as a photocatalytic material and these studies produced a series of intriguing results. For example, oxygen vacancies have been correlated with catalytic activity [8], suggesting that coordinatively unsaturated Ti may serve as the catalytic site, but STM studies [9] have shown that oxygen vacancies frequently, if not exclusively, occur in pairs accompanied by an adjacent Ti vacancy. Theoretical studies have shown that the introduction of such an oxygen vacancy actually displaces the Fermi level to the conduction band minimum (cbm) [10].

The primary aim of this paper is to review recent investigations of the influence of dopants on the optical properties of $TiO_2$ polymorphs. To the best of our knowledge there is no current review, although there is an excellent feature article by Serpone [11], and several articles with

especially strong review sections. Among these are [12–15]. Another valuable resource is a special issue of the *International Journal of Photoenergy* on the subject of "Doped $TiO_2$ Nanomaterials and Applications" [16]. There is also a special issue of *Chemical Physics* on "Doping and Functionalization of Photoactive Semiconducting Metal Oxides" [17], which contains many relevant papers. We will focus on the most recent results, citing older works to place the recent results in context. We begin by comparing and discussing the $TiO_2$ polymorphs. We then review the results of recent doping efforts and tabulate the findings by $TiO_2$ polymorph, dopant, effect on the band gap, effect on photocatalytic activity, and so forth. We also present a simple qualitative picture of the $TiO_2$ electronic structure and support it with first-principles calculations. This picture provides a framework for a general understanding of the $TiO_2$ electronic structure with which the tabulated results may be interpreted.

## 2. Polymorphs of $TiO_2$

The structure and properties of $TiO_2$ polymorphs could themselves be the subject of a review and it is impractical to attempt a full review of these topics here. Nevertheless, some background provides a useful foundation for describing the doping studies. The three most widely known polymorphs of titanium dioxide are rutile (tetragonal), anatase (tetragonal), and brookite (rhombohedral). These can exist as bulk structures and nanoparticles. Rutile has six atoms in a unit cell with each titanium atom bonded to six oxygen atoms and each oxygen atom bonded to three titanium atoms. The anatase structure is similar, but slightly more distorted than rutile. Two of the titanium-oxygen bonds are much longer than the other four bonds and the O–Ti–O bond angles deviate more from 90° than in rutile. Brookite has an orthorhombic cell. Though the interatomic distances and O–Ti–O bond angles are similar to those of rutile and anatase, there are six different Ti–O bonds ranging from 1.87 to 2.04 Å in length. There are also twelve different O–Ti–O bond angles ranging from 77° to 105° [26]. Surprisingly, brookite and rutile are structurally similar because both phases are formed by straight polyhedron chains linked through three different corners of the unit cell, but the linking of polyhedron chains occurs through cis bridges in brookite [42]. More complete descriptions of the bulk structures may be found in [24, 26].

The polymorphs of titanium dioxide find different uses. For instance, the rutile phase is usually used in high-grade, corrosion-protective white coatings and paint, or in plastics, rubber, leather, sun-block lotion, and paper due to its high refractive index. The anatase phase has excellent optical and pigment properties due to its electronic structure and it is used as an optical coating and photocatalyst. Applications of brookite are limited because it is uncommon and has historically been difficult to synthesize. It has similar general chemistry and similar physical properties (such as color and luster) to rutile. There has recently been a surge of interest in producing high purity $TiO_2$ in the brookite structure because there are experimental clues that it may posses superior photocatalytic properties [43].

Several measurements and calculations of the crystalline lattice parameters for the different polymorphs of $TiO_2$ are collected in Table 1. Note that, in general, the modern first-principles methods give reliable predictions of the lattice constants, that is, predicted values in very good agreement with those from neutron and X-ray diffraction experiments. By contrast, predictions of the bulk modulus vary widely. This finding is perhaps unsurprising because derivative properties are typically more difficult to converge than total energy properties. A particularly intriguing result is the anomalously low predicted value of the bulk modulus for brookite reported by Mo and Ching [26] (relative to the experimentally determined value [41]). Mo and Ching made the plausible attribution of this apparent softness to the distorted nature of the $TiO_6$ octahedra in brookite. Alternatively, one could dismiss this value as an artifact of the computational methodology, save for the fact that using the same methodology, Mo and Ching obtained a very accurate prediction of the bulk modulus for rutile (again by comparison with the experimentally determined value [34]).

Measurement of the band gap (bg, $E_g$) in doped titania is typically by UV-Vis adsorption spectroscopy or by applying the Kubelka-Munk treatment to diffuse reflectance spectra. A comparison of these approaches is given in [44]. Computational predictions generally greatly underestimate the band gap in $TiO_2$. This is because most theoretical studies have employed Density Functional Theory (DFT) in the Local Density Approximation (LDA) [45], which typically underestimates the band gap in semiconductors and insulators by 30–50% [46]. Despite the significant underestimation, predictions of $E_g$ for the three common phases of $TiO_2$ generally follow the experimentally observed trend $E_g$ (rutile) < $E_g$ (anatase) < $E_g$ (brookite) when all three values are computed with a consistent set of approximations [26]. There are a few notable exceptions to the general rule of theoretical calculations underestimating the band gap. Beltrán et al. [32] followed the traditional approach for crystalline materials, carrying DFT calculations on unit cells of an infinitely periodic solid using periodic boundary conditions, but employed an atomic-orbital basis and the B3LYP correlation functional, which are techniques more commonly employed in molecular quantum chemistry. (Plane waves and LDA are more common in solid state calculations.) As shown in Table 1, their predicted values of $E_g$ are in much better agreement with experimental results than traditional LDA calculations. Dai and Huang [36] achieved good results with a 13% HF hybrid functional, as did Zhang and colleagues [47]. Harrison and colleagues have discussed the use of hybrid functionals for band gap prediction [48] and demonstrated their success on mixed oxide systems [49, 50]. Such works might be taken to imply that the LDA and Generalized Gradient Approximation (GGA) [51–54] functionals traditionally used in periodic-boundary DFT studies are at the root of the underestimation of the band gap, but Wang, Lewis and coworkers achieved good agreement with experiment in the calculation of $E_g$ by employing LDA, but a localized atomic orbital basis [31, 55]. With the increasing importance of accurate prediction of optical properties for rapid computational screening of

Table 1: Crystalline lattice parameters, bulk modulus (B), and band gap $E_g$ of $TiO_2$ polymorphs. HF: Hartree-Fock, PBE [18], BLYP [19, 20], B3LYP [21, 22], OLCAO: Orthogonalized Linear Combination of Atomic Orbitals, FLAPW: full potential linearized augmented plane wave method.

| | a (Å) | b(Å) | c (Å) | B (GPa) | $E_g$ (eV) | Notes | Ref. |
|---|---|---|---|---|---|---|---|
| Rutile $P4_2/mnm$ | 4.634 | — | 2.963 | 204 | — | PBE | [23] |
| | 4.546 | — | 2.925 | 249 | — | LDA | [23] |
| | 4.679 | — | 2.985 | 200 | — | BLYP | [23] |
| | 4.58666 | — | 2.95407 | — | — | neutron | [24] |
| | 4.5929 | — | 2.9591 | — | — | X-ray | [25] |
| | ″ | ″ | ″ | 209.34 | 1.78 | OLCAO | [26] |
| | 4.568 | — | 2.926 | — | 1.68 | LDA | [27] |
| | 4.579 | — | 2.989 | — | — | HF | [28] |
| | 4.548 | — | 2.944 | — | — | LDA | [28] |
| | 4.623 | — | 2.987 | — | — | GGA | [28] |
| | 4.567 | — | 2.932 | — | 2.00 | LDA | [10] |
| | 4.594 | — | 2.959 | — | 1.9 | GGA | [29] |
| | 4.653 | — | 2.965 | 240 | 2.0 | LDA | [30] |
| | 4.5729 | — | 2.9511 | 206 | 3.05 | OL-LDA | [31] |
| | — | — | — | — | 3.24 | B3LYP | [32] |
| | — | | — | — | 2.0 | LDA | [33] |
| | — | — | — | 210 | — | — | [34] |
| | — | — | — | — | 3.0 | — | [35] |
| | — | — | — | — | 3.07 | 13% HF | [36] |
| | — | — | — | — | — | — | |
| Anatase $I4_1/amd$ | 3.786 | — | 9.737 | 176 | — | PBE | [23] |
| | 3.735 | — | 9.534 | 199 | — | LDA | [23] |
| | 3.828 | — | 9.781 | 178 | — | BLYP | [23] |
| | 3.78216 | — | 9.50226 | — | — | neutron | [24] |
| | 3.692 | — | 9.851 | — | 2.00 | FLAPW | [33] |
| | 3.783 | — | 9.514 | — | — | X-ray | [25] |
| | ″ | ″ | ″ | 272.11 | 2.04 | OLCAO | [26] |
| | — | — | — | 200.2 | | B3LYP | [32] |
| | — | — | — | — | 3.26 | LO-LDA | [37] |
| | | — | — | 179 | — | — | [38] |
| | — | — | — | — | 3.34 | — | [39] |
| | — | — | — | — | 3.58 | 13% HF | [36] |
| | | — | — | — | | | |
| Brookite Pbca | 9.184 | 5.447 | 5.145 | — | | X-ray | [40] |
| | ″ | ″ | ″ | 137.32 | 2.2 | OLCAO | [26] |
| | 9.276 | 5.502 | 5.197 | 220 | 3.78 | B3LYP | [32] |
| | — | — | — | 255 | — | — | [41] |
| | — | — | — | — | 3.4 | — | [39] |

proposed new materials, these promising approaches appear to merit further exploration.

The above-mentioned paper by Wang and colleagues [55] is especially fascinating. They apply an electronic state quantum entropy approach to define a "quantum entropy" for a state. Using this entropy estimate, Boltzmann statistics is applied to estimate number of atoms assessable to that state. This gives a measure of how localized a state is. They find that while the bg is relatively independent of doping concentration (as reported by others, vide infra) impurity states are much more localized at low dopant concentration, so hole mobility is likely low, explaining low catalytic efficiency. As noted by In and coworkers [56], "merely inducing visible light absorption does not guarantee photocatalytic activity."

Lack of photocatalytic activity can result from rapid electron-hole recombination occurring before the electron and/or hole species have time to carry out catalytic reduction/oxidation [2]. High hole mobility is therefore another key to good activity, and the ability to predict this property through calculations is important to materials screening and design. The introduction of a dopant can influence the

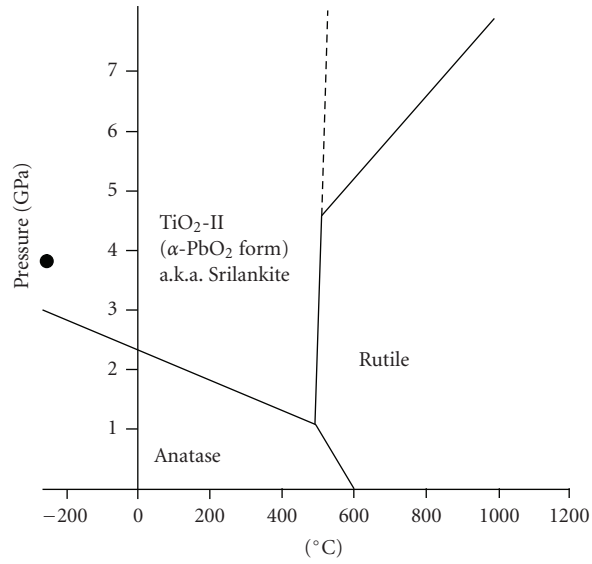


Figure 1: Composite phase diagram for $TiO_2$. The anatase/$TiO_2$-II, anatase/rutile, and $TiO_2$-II/rutile phase boundaries are taken from Ren et al. [71]. The $TiO_2$-II/rutile phase boundary at high temperatures and pressures is taken from Withers et al. [58]. The filled point shows the 0 K anatase-to-brookite transition pressure estimated by Beltrán et al. [32].

recombination rate in several ways. First, a dopant can favor the formation of smaller particles. For example, Kato et al. [59] have found that La doping of an NiO/$NaTaO_3$ photocatalyst leads to catalytic nanoparticles that are ten times smaller than undoped particles and increases photocatalytic activity by a factor of nine. Similar results for doped titania are noted later in this paper. Smaller particles have larger surface-to-volume ratios and consequently enhanced quantum yield because the paths by which electrons and holes generated in the "bulk" migrate to the surface are shorter. Shortening the migration paths decreases the probability that the electrons and holes will recombine before reaching the surface where catalysis is carried out. One mechanism by which the introduction of a dopant can favor the formation of smaller particles is by stabilizing the surface [60]. Smaller particles also present greater surface area, which accentuates catalysis. Any processing that reduces surface area generally decreases activity [61]. The influence of quantum confinement on the electronic structure can change the activity as well [62, 63]. A second mechanism by which the introduction of a dopant can influence the recombination rate is by electronic state symmetry breaking. Radiative decay paths that are symmetry forbidden in the pure material may have a nonnegligible transition moment in the doped material because the presence of the dopant breaks the symmetry of one of the states involved [57, 64, 65]. A third way that the introduction of a dopant can influence the recombination rate is by introducing an impurity electronic state, or trapped defect [66], that can serve as a facile recombination center [67]. On the other hand, metals such as Ni and Pt are also sometimes added as a surface modification to inhibit recombination of electron/hole pairs. A metal particle on the surface acts as an electron trap, increasing the physical separation between the electron and hole, thereby preventing recombination [2]. Additionally, a metal dopant may increase hole mobility, thereby diminishing the recombination rate. For example, Obata et al. showed that the introduction of Ta as a dopant adjacent to an N dopant increases dispersion of dopant band, presumably increasing mobility of holes [68]. One promising application of metals to increase catalytic activity (though not necessarily by decreasing the recombination rate) capitalizes on interfacial charge transfer between metals in the oxide bulk and others grafted to the surface [69]. The metal centers grafted to the surface serve as catalytic reduction sites. These are activated by photoinduced charge transfer from metal centers in the oxide bulk. Irie et al. were able to achieve quantum yields as high as 17% for photocatalytic decomposition of 2-propanol using this approach [70].

The relative stability of the polymorphs of $TiO_2$ has been a matter of some investigation. Total energy calculations by Lazzeri et al. [23] find anatase to be more stable than rutile by 0.02–0.12 eV/formula unit (depending on the specific $V_{xc}$ used). Beltrán et al. [32] reported internal energy versus unit cell volume curves for anatase, rutile and brookite. Visual inspection of their Figure 3 shows anatase to be more stable than rutile by ~0.14 eV/formula unit, in good agreement with the work of Lazzeri at al. Beltrán et al. [32] found brookite to be intermediate between anatase and rutile in stability. Such total energy calculations are 0 K, zero pressure calculations. Nevertheless, they provide estimates of the 0 K intercept points of the phase boundaries in the P-T phase diagram, which are often good approximations for atmospheric pressure as well. A composite phase diagram is shown in Figure 1, where it can be seen that anatase is the "regular" phase, consistent with the theoretical calculations noted previously. Rutile is the high-temperature high-pressure phase and $TiO_2$-II is the high-pressure low-temperature phase. Several of the boundaries are taken from Ren et al. [71]. By scanning and digitizing their phase diagram we find the following expressions for the phase boundaries. The anatase/$TiO_2$-II phase boundary is given by

$$P = -0.0026T + 2.31, \quad (1)$$

where $T$ is in degrees Celsius and $P$ in GPa. The anatase/rutile phase boundary is given by

$$P = 0.009T + 5.44. \quad (2)$$

The $TiO_2$-II/rutile phase boundary is given by

$$P = 0.14T - 69.4. \quad (3)$$

Withers et al. [58] give the $TiO_2$-II/rutile phase boundary at high temperatures and pressures as

$$P = 0.0065T + 1.29, \quad (4)$$

which is also shown in Figure 1. Based on first principles calculations, Beltrán et al. [32] estimated the anatase-to-brookite transition at 3.8 GPa, shown by the filled point

in Figure 1. Given that anatase and brookite are thought to be low-temperature low-pressure forms with Srilankite forming under high pressure [71], the theoretically predicted anatase-to-brookite transition pressure appears to be slightly too high, perhaps due to neglect of entropic considerations. Beltrán et al. [32] estimate the transition pressure for the rutile-to-brookite transition at 6.2 GPa, and Swamy et al. [72] estimate the transition pressure for the rutile-to-$TiO_2$-II transition at 27.8 GPa, although the composite phase diagram suggests that rutile is itself metastable at low temperatures. The phase diagram shown in Figure 1 is certainly very incomplete. It is unclear if there is a region of P-T space where brookite is the doninant phase. Also, there are apparently a series of high pressure forms in addition to $TiO_2$-II, including baddeleyite ($\alpha$-$ZrO_2$ structure) and cotunnite ($PbCl_2$ structure) as discussed by Withers et al. [58] and Swamy et al. [72]. These structures appear to be principally of interest to the geophysics community because their appearance in metamorphic rock can give information about the magnitude of pressures that were present during the geologic past [58]. Further thermochemical modeling studies of $TiO_2$ under oxygen atmosphere have been reported by Waldner and Eriksson [73].

One complicating feature of the phase behavior of $TiO_2$ is that the dominant phase depends not only on temperature and pressure, but also on particle size. For example, it is observed that nanoparticles of $TiO_2$ prefer the anatase structure when the characteristic particle size is less than ca 14 nm [37], even when heated to high temperature. The presence of this third independent variable (particle size) in the phase diagram is due to differences among the surface energies of the various polymorphs. For sufficiently small particles, surface energy is a sufficiently large fraction [74] of the free energy of formation that differences in surface energy dictate the favored polymorph. A detailed theoretical investigation of rutile surfaces, which includes a rather comprehensive set of references, has been presented by Perron and colleagues [75]. Computed surface energies for various surface exposures of the different polymorphs of $TiO_2$ are collected in Table 2. Cursory inspection does not show any significant surface energy preference for the anatase form, but it is important to recognize that any real nanoparticle will reveal several surface exposures of different areas. The molecular dynamics (MDs) work of Naicker et al., which takes into account the entire surface of the nanoparticle, clearly shows the energetic preference for anatase over rutile [76].

The $TiO_2$ polymorphs in nanoparticulate form (characteristic particle size < 100 nm) find similar application to their bulk (characteristic particle size > 100 nm) counterparts, but nanoparticles offer numerous advantages, such as higher surface area for catalytic applications, and therefore are the focus of considerable recent synthetic efforts. A review of these synthetic approaches is beyond the scope of this paper, but it is important to note that the dominant phase produced is often quite sensitive to the reaction conditions. For example, rutile particles are obtained by using titanium (IV) isopropoxide in nitric acid at pH of 0.5 [77] or titanium (IV) chloride in an aqueous/alcohol solution of hydrochloric acid [78]. Anatase nanoparticles are formed also from titanium (IV) isopropoxide, but in acetic acid [79], and the use of nitric acid produces a mixture of phases [80]. Brookite is the least common polymorph, plausibly because it is the farthest from equilibrium under ambient conditions, at least according to the phase diagram shown in Figure 1. Nevertheless, owing to its promising optical and photocatalytic properties [43], it has been the target of significant recent synthetic effort [42, 81, 82]. The observed sensitivity to reaction conditions suggests that it should ultimately be possible to obtain good control over $TiO_2$ nanoparticle synthesis.

Table 2: Surface energies for $TiO_2$. Details of specific surface exposure are given in Ref. cited.

| Surface | ergs/cm$^2$ | Notes | Ref. |
|---|---|---|---|
| *rutile* | | | |
| (110) oxygen terminated | 892 | LDA | [83] |
| | 524 | FLAPW | [92] |
| | 840 | LDA | [23] |
| | 350 | PBE | [23] |
| | 830 | PBE + U | [93] |
| | 890 | LDA | [94] |
| | 540 | GGA | [75] |
| (110) Ti–O terminated | 4245 | FLAPW | [92] |
| | 2250 | DFT | [95] |
| (001) | 1876 | LDA | [94] |
| | 132 | GGA | [75] |
| (100) | 1121 | LDA | [83] |
| | 1197 | LDA | [94] |
| | 760 | GGA | [75] |
| (101) | 108 | GGA | [75] |
| Nanoparticle[(a)] | 2620 | MD | [76] |
| *Anatase* | | | |
| (101) | 840 | LDA | [23] |
| | 490 | PBE | [23] |
| (100) | 960 | LDA | [23] |
| | 580 | PBE | [23] |
| | 1540 | DFT | [95] |
| (001) | 1380 | LDA | [23] |
| | 980 | PBE | [23] |
| (110) | 1150 | PBE | [23] |
| Nanoparticle[(a)] | 2180 | MD | [76] |
| *Brookite* | | | |
| (100) | 880 | GGA | [96] |
| (010) | 770 | GGA | [96] |
| (001) | 620 | GGA | [96] |
| (110) | 850 | GGA | [96] |
| (011) | 740 | GGA | [96] |
| (111) | 720 | GGA | [96] |
| Nanoparticle[(a)] | 2170 | MD | [76] |

[(a)]6 nm diameter.

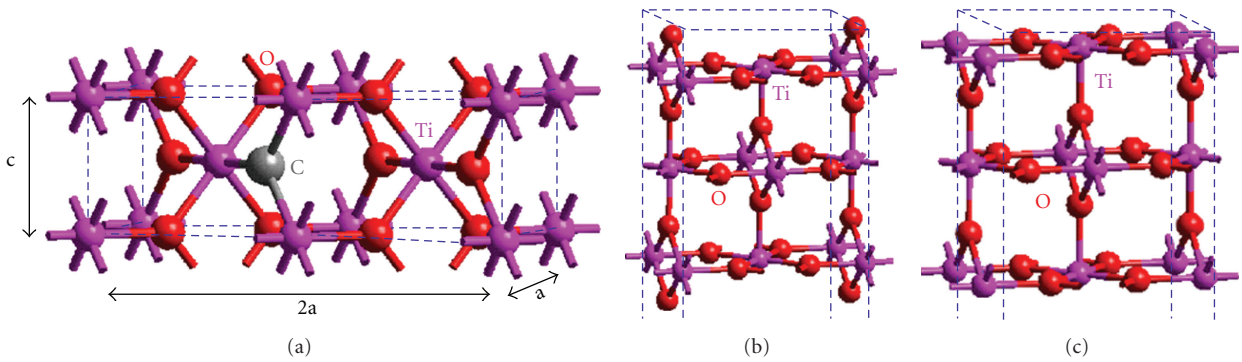


Figure 2: Unit cells used in present calculations. (a) $2 \times 2 \times 1$ supercell ($Ti_4O_7C$) with substitutional carbon doping. (b) Stoichiometric (110) surface, (c) nonstoichiometric Ti–O termination of the (110) surface.

## 3. Qualitative Interpretive Model of Doped-$TiO_2$

*3.1. Structure Models.* To help describe the influence of dopants on the optical properties of titania, we present a simple qualitative model of its electronic structure (vide infra). In an effort to place this qualitative model onto a firmer foundation, we have applied first-principles density-functional calculations. We investigated the electronic and structural properties for $TiO_2$ bulk (rutile) and its (110) surface, which is thought to be dominant in catalytic applications [83]. For studies of the bulk we employed $2 \times 1 \times 1$ supercells of stoichiometry $Ti_4O_8$, (as shown in Figure 2(a)) $Ti_4O_7X$ for substitutional doping and $Ti_4O_7XY$ for substitutional + interstitial codoping. The cells used for the surface studies are shown in Figures 2(b) and 2(c). It is to be emphasized that these calculations are intended solely to reinforce the qualitative discussion of the electronic structure of doped titania and its stability upon doping. For an accurate quantitative description of the electronic structure the reader is referred to the references cited.

*3.2. Theoretical Methods.* The calculations presented here to support the simple qualitative model of doped-$TiO_2$ electronic structure were based on first-principles density functional theory [45]. Structural relaxations, total energies, and band structure were computed using ultrasoft pseudopotentials (PP) [84] to describe the electron-ion interactions and plane waves to describe the valance electrons. The CASTEP [85] and DACAPO [86] codes were employed in this study. Structures optimized with one code were invariably found to be well converged when optimized with the other code. Interband transition energies in doped $TiO_2$ were computed by empirical rescaling based on a best-fit linear correlation between experimental and computed results (described in more detail below). The GGA form of the exchange-correlation was used in all cases [87]. A 7-layer symmetrical slab with 14 Å vacuum spacing between slabs was used for the surface calculations, which produced relaxations in quantitative agreement with previous experimental [88] and theoretical [10] results. No appreciable sensitivity of the results reported herein was found with respect to increasing; the plane wave cutoff energy, the number of k-points, or in the case of the surface calculations, the slab thickness. This is consistent with earlier theoretical work showing convergence with respect to slab thickness at six layers [89].

Table 3: Energies (eV) for formation ΔE of several doped species from stoichiometric $TiO_2$ and the pure element, fully optimized cell parameter $\gamma$, (note that $\alpha = \beta = 90$ even after full unit cell optimization) and volume change (%) upon doping.

| Doped species | ΔE | $\gamma$ | ΔV |
|---|---|---|---|
| $Ti_4O_7B$ | 8.3 | 94 | 5.9 |
| $Ti_4O_7C$ | 8.9 | 92 | 3.4 |
| $Ti_4O_7N$ | 5.3 | 90 | 1.6 |
| $Ti_4O_7F$ | 0.18 | 92 | 2.6 |
| $Ti_4O_7BF$ | 3.5 | 98 | 10.2 |
| $Ti_4O_7Ga$ | 6.4 | 97 | 9.3 |

Using the above methods, we relaxed the rutile structure to obtain lattice constants and atomic positions (force < 0.01 eV/a.u. per atom). The optimized parameters are a = 4.599 Å, c = 2.974 Å. This is in essentially exact agreement with experimentally measured values of a = 4.594 Å, c = 2.979 Å [90]. See also Table 1.

Formation energies are here approximated by the change in total energy according to the equation

$$Ti_4O_8 + \frac{1}{n}X_n + \frac{m}{2}F_{2(g)} \longrightarrow Ti_4O_7XF_m + \frac{1}{2}O_{2(g)}. \quad (5)$$

Here "$X_n$" is a primitive unit cell of the corresponding dopant in its elemental form ($B_{(s)}$, $C_{(s)}$, $N_{(g)}$, or $F_{(g)}$). Note that the B-doped material has a formation energy comparable to that of the C-doped material. In most cases considered here $m = 0$, but in the case of codoping with F discussed below ($m \neq 0$), one of the dopant atoms is placed interstitially at the nominal fractional coordinates (0.5, 0.5, 0.5). Combining tabulated integrated third law entropies for the gaseous species with the computed total energies to estimate changes in *free energy*, a technique discussed in [91], does not qualitatively change the predicted reaction spontaneity at 300 K. Given in Table 3 are the energies for

formation of the doped materials from stoichiometric $TiO_2$ and the pure elemental form of the dopant.

Since DFT with (semi-) local functionals typically underestimates the band gap, and since the unoccupied (conduction band) states are not self consistent, further manipulation is required to predict the band gap. Perhaps the most theoretically justifiable approach would be to carry out GW [97] calculations, which have been shown to rectify the underestimation of the band gap [46]. While desirable, such calculations are generally impractical. As discussed above, DFT with hybrid functionals, especially when used in combination with an atomic orbital (AO) basis, appears promising for bg estimation when applied by the hands of experienced practitioners, but has not yet been distilled to a standard protocol. In lieu of a theoretically rigorous method like GW, a common approach to correct the band gap is to use a "scissors operator" whereby the entire conduction band is shifted up in energy so that the cbm lies above the valance band maximum (vbm) by exactly the experimentally observed bg. One shortcoming of this approach is that in the case where isolated states lie within the band gap, the scissors operator leaves some uncertainty as to how to shift these states. For example, a scissors operator of 1.0 [98], 1.1 eV [99–101], or 1.25 eV [102] works well for pure $TiO_2$, but would exaggerate the bg in the doped case. Here we have applied an empirical approach. By fitting computed and experimental data to a straight line we can estimate the experimental onset ($E_{\text{fit}}$) based on a computed interband energy gap ($E_{\text{comp}}$). Using the data highlighted in bold in Table 4, the best-fit line is

$$E_{\text{fit}} = 1.2258 * E_{\text{comp}} + 0.8052 \quad \text{(in eV)}. \tag{6}$$

*3.3. Qualitative Model of the Band Structure.* Qualitatively, in the band structure of $TiO_2$, the valance band is principally oxygen $2p$ in character and the conduction band is principally Ti $3d$ & $4s$ in character [26, 103]. In rutile, the conduction band minimum is ca 3 eV above the valance band maximum. In the anatase form the band gap (bg) is slightly greater (see Table 1). Roughly speaking, the greater bg in anatase arises because anatase has a lower material density than rutile. With lower density, the atom-atom distances are slightly greater, resulting in weaker coupling and less band dispersion. With less dispersion, the vbm and cbm are slightly farther apart. This rough argument extends to the brookite form as well. In rutile, the Ti atoms reside in an octahedral environment splitting the $3d$ atomic orbitals so that $d_{xy}$, $d_{xz}$, and $d_{yz}$ reside near the bottom of the cb while $d_{z^2}$ and $d_{x^2-y^2}$ are higher in the cb [104]. The same general features are found in the anatase electronic structure, but the splittings are more complicated on account of the slight distortion of the octahedral environment in the anatase structure [33]. More extensive discussion may be found in Sorantin and Schwarz [104] (rutile) and Asahi et al. [33] (anatase).

Since oxygen has six valance electrons and titanium four, in the atomic limit each stoichiometric $TiO_2$ unit contributes two filled oxygen $2p$ orbitals, four half-filled oxygen $2p$ orbitals, and four titanium valance electrons in Ti $3d$ & $4s$. In $TiO_2$, the four titanium valance electrons drop into the half-filled oxygen $2p$ orbitals. This leaves the Ti $3d$ & $4s$ orbitals empty to form the conduction band and fills O $2p$ orbitals to form the valance band. Figures 3(a) and 3(b) show a schematic comparison of the band structure of the stoichiometric termination of $TiO_2$ with that in the presence of an oxygen vacancy. When an oxygen atom is removed, three oxygen $2p$ orbitals are removed, but only four electrons. The remaining two electrons that occupy these orbitals in $TiO_2$ are from Ti. In the absence of the oxygen $2p$ they must reside in Ti $3d$ orbitals. The lowest such orbitals are at the cbm. It has long been thought [105] that the extra electrons localize on two adjacent Ti atoms, reducing them to Ti(III). This has been confirmed by detailed theoretical analysis [93]. The progression of the dopant band(s) with respect to the valance band as the atomic number of the dopant is changed is depicted qualitatively in Figure 3 and semiquantitatively in Figure 4 and is elaborated upon below when the specific dopants are discussed. The band structure "spaghetti" plots shown in Figure 4 are directly from the GGA calculations and not influenced by (6).

*3.4. Associated O and Ti Vacancies.* As a consequence of the above, oxygen vacancy formation has a large associated energy cost, nominally the cost of moving two electrons from the vbm to the cbm. This is in qualitative agreement with the large computed value. (Reliable recent calculations give 4.2 [14, 106] or 4.42 eV/vacancy [93].) In fact, titania is generally nonstoichiometric [107], $TiO_{2-x}$, and consequently n-type. Surface oxygen vacancies are formed relatively more easily, varying between 3.12 and 3.73 eV/vacancy depending on the surface plane exposed [93]. Surface oxygen vacancies are important because they have been correlated with catalytic activity [8], suggesting that coordinatively unsaturated Ti may serve as the catalytic site. In fact, it has been suggested that enhanced catalytic activity in doped $TiO_2$ may arise, at least in some cases, from the presence of the dopant inducing oxygen vacancies [108]. STM studies [9] have shown that oxygen vacancies frequently, if not exclusively, occur in pairs accompanied by an adjacent Ti vacancy, and that adsorbed oxygen molecules can mediate the diffusion of vacancies [109]. We can now understand why oxygen vacancies are frequently accompanied by adjacent Ti vacancies. If a surface oxygen is removed, and an adjacent Ti, it is no longer necessary to place Ti valance electrons into the conduction band. In other words, the presence of an adjacent Ti vacancy stabilizes an oxygen vacancy [92]. In fact, visual inspection of published STM images shows Ti and oxygen vacancies occurring in stoichiometric $TiO_2$ groups [9]. Detailed discussion of $TiO_2$ surface defects can be found in [110–112].

An especially detailed presentation of the chemistry of surface vacancies has been given very recently by Morgan and Watson [93]. They have used crystal field arguments with great success in understanding surfaces with vacancies. For example, Ti atoms in rutile $TiO_2$ are nominally in an octahedral ($O_h$) coordination environment. Crystal field theory holds that in this environment the t-states arising

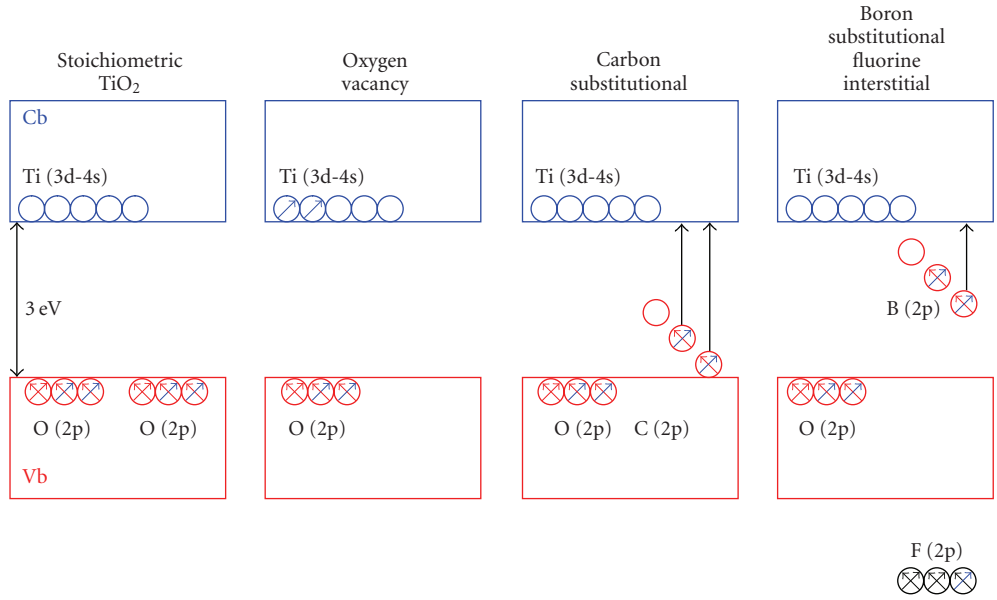


FIGURE 3: Schematic representation of the electronic structure. (a) Far left: $TiO_2$, (b) left center: with oxygen vacancy, (c) right center: with carbon doping, (d) far right: with B and F codoping. The valance band is principally oxygen 2*p* in character. The conduction band is principally Ti 3*d* & 4*s* in character. In the atomic limit, each $TiO_2$ unit contributes two filled oxygen 2*p* orbitals, four half-filled oxygen 2*p* orbitals, and four titanium valance electrons. In the pure material, (far left) the four titanium valance electrons fill the vacant oxygen 2*p* orbitals. When an oxygen atom is removed, (center left) three oxygen 2*p* orbitals are removed, but only 4 electrons. The remaining two electrons are forced to reside in Ti 3*d* orbitals. Upon substitution of C for O, (center right) the carbon 2*p* bands "float up" into the band gap due to weaker nuclear-electron interaction. Onsets in the photoabsorption spectrum are seen corresponding to transitions from both occupied carbon 2*p* bands to the conduction band. B-F codoping (far right) fills the half-full F-2*p* orbital with a large energy benefit.

from the 3*d*-orbitals of Ti lie at a lower energy than the e-states. This is consistent with the qualitative description of rutile electronic structure presented by Sorantin and Schwarz [104]. In a tetrahedral coordination environment, however, the e-states arising from the 3*d*-orbitals of Ti lie at a lower energy than the t-states. This is important because Ti atoms adjacent to a surface oxygen vacancy on the (101) exposure are four-coordinated, two of the neighboring oxygen atoms that are normally present in the bulk being missing. The local structure such Ti atoms therefore distorts toward tetrahedral ($T_d$) coordination. As shown in Figure 5, distortion from $O_h$ to $T_d$ gradually increases the energy of the t-states and decreases the energy of the estates. Because the two Ti atoms adjacent to a surface oxygen vacancy on the (101) surface are not symmetry equivalent, the degree of distortion is different. The occupied states therefore lie at slightly different energy as shown by the solid and filled circles in Figure 5. This is the origin of the splitting in the defect state for the defective (101) surface [93].

*3.5. Movement of Fermi Energy from vbm to cbm.* The above qualitative description also explains the difference between the band structure of the stoichiometric termination of $TiO_2$ and the nonstoichiometric "Ti–O" termination [10]. The dominating feature is the displacement of the Fermi level from the vbm to the cbm in the latter case. This displacement may be understood by recognizing that the Ti–O terminated surface is effectively equivalent to two surface oxygen vacancies per unit cell, forcing Ti valence electrons into the conduction band. As shown in Table 2, the computed surface energy of the Ti–O termination ($4245\ erg/cm^2$) is nearly an order of magnitude larger than that of the stoichiometric termination ($524\ erg/cm^2$). The high surface energy in the Ti–O terminated case is principally due to the displacement of four electrons per unit cell from the valence band to the conduction band.

## 4. Doped $TiO_2$

Computed and experimental optical transition energies for variously doped rutile and anatase $TiO_2$ are collected in Table 4, which is annotated with comments about the influence of the dopant on photocatalytic activity.

*4.1. Doping by Group V-A Elements.* Since the early success of Asahi et al. [6], nitrogen-doping of $TiO_2$ has been studied quite extensively and it remains one of the most promising approaches to optimizing the bg and photocatalytic activity of titania. While synthetic strategies are not reviewed here, numerous approaches have been taken and an extensive set of references may be found in [113].

As noted by Livraghi et al. [113], for rational and systematic use of N-doping to optimizing the bg and photocatalytic activity of titania, "one needs to distinguish between the inert byproducts of the chemical preparation, unavoidably present in the solid, and species which are playing an effective

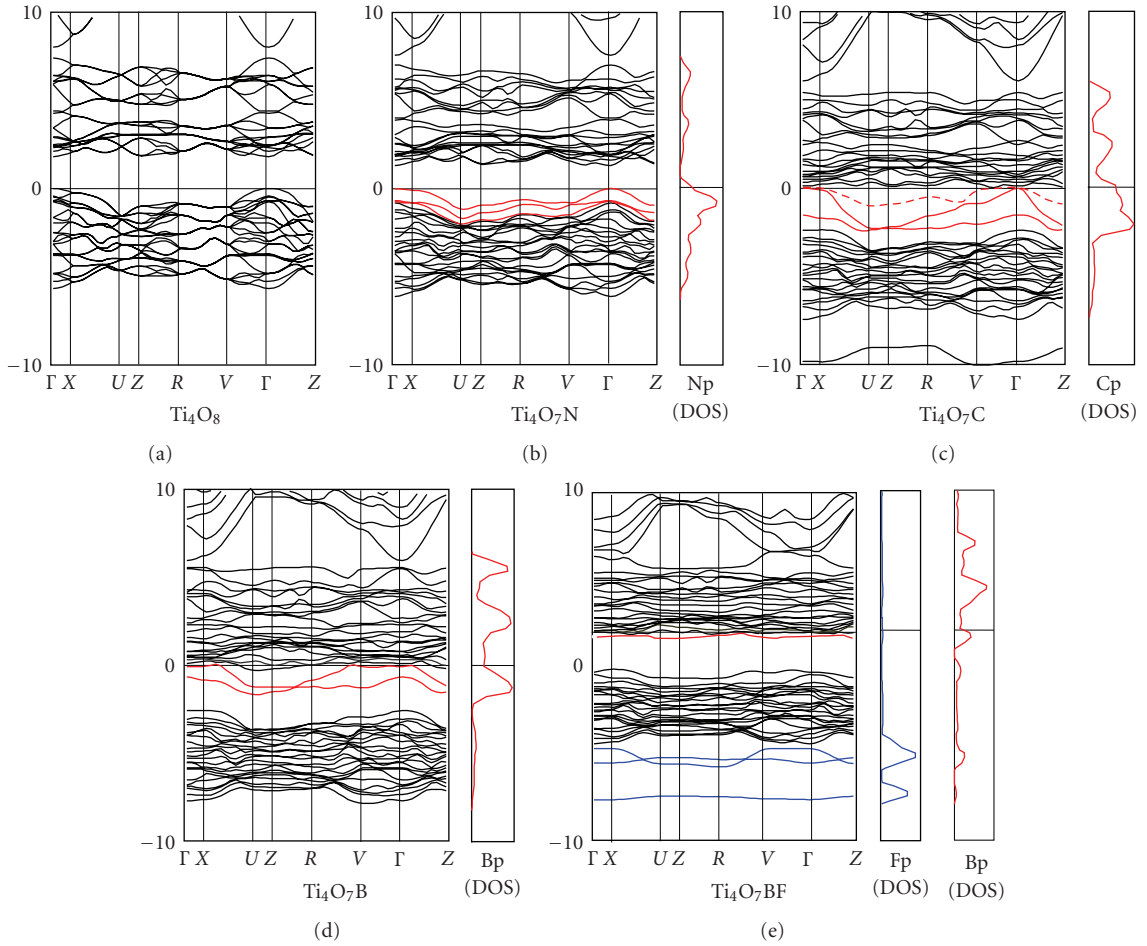


FIGURE 4: Band structures and DOS for substitutional doping within a 2×1×1 supercell. (a) Pure rutile $TiO_2$. (An atypical path is shown for more direct comparison to the doped species.) (b) N-doping: the three $2p$-bands are occupied by five electrons. (c) C-doping: the $2p$-bands are occupied by four electrons. (d) B-doping: two $2p$-bands are occupied by three electrons. (e) B-substitutional, F-interstital. Bands of $p$-character nominally arising from the substitutional dopant are identified by the projected density of states, and shown in solid red where they are occupied. Bands shown in blue are nominally due to interstitial F.

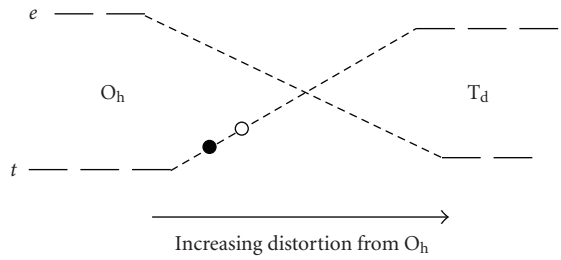


FIGURE 5: Schematic representation of the interchange between the t- and e-states arising from the five *nd* atomic orbitals is the local environment and is distorted from octahedral to tetrahedral. Sites with different degrees of distortion will give rise to bands at different energies as shown by the filled and open circles.

role in the visible light adsorption and molecular (photo) activation." This is not always clear. For example, it has been suggested that N-doping leads to visible light adsorption by narrowing the bg [6], or by introducing an impurity electronic state within the bg [114]. The picture is further complicated by the observation of differences between rutile and anatase. The bg in the former has actually been reported to be blue shifted by N-doping [115]; whereas in the latter it is red shifted, except in some codoped cases [13]. Another complication is the coexistence of oxygen vacancies. Wang and Doren [108] predicted that N substituting for O in anatase introduces states above the vbm, but furthermore, oxygen vacancies introduce states near the cbm. The presence of N-doping can stabilize these oxygen vacancies [116]. The band structure for N-doped anatase, complementary to the case of N-doped rutile shown here in Figure 4(b), can be found in [98].

The qualitative difference in the effect of N-doping on the bg between rutile and anatase was finally resolved by theory [117]. As noted above, band dispersion is greater in rutile than in anatase, principally due to higher material density in the former. In the atomic limit, nitrogen $2p$ orbitals are higher in energy than oxygen $2p$ orbitals because the nuclear charge is smaller. When a nitrogen atom replaces

Table 4: Comparison of experimental and computed absorption onsets with notes about photocatalytic activity. Since direct comparison of improvements in catalytic efficiency between catalysts is difficult unless the same test reactions are used, quantitative notes about photocatalytic activity are relative to other measurements reported in the same reference. Values used in fitting (6) are shown in boldface. Values in parenthesis are prior to empirical scaling.

| Composition | Activity notes | $E_g$ (eV) | Ref. |
|---|---|---|---|
| | *rutile* | | |
| Ishihara Sangyo PT-101 | No photodecomposition of 2-propanol or methylene blue above 450 nm | **3.03** | [140] |
| 1.6 wt% S substitutes for Ti, calcined 700 C | | 2.94 | [140] |
| 1.6 wt% S substitutes for Ti, calcined 600 C | | 2.31 | [140] |
| 1.6 wt% S substitutes for Ti, calcined 500 C | Photodecomposition of 2-propanol and methylene blue above 450 nm | 2.20 | [140] |
| FLAPW undoped | | 2.34 | [140] |
| FLAPW S-doped | | 0.975 | [140] |
| Undoped | | 1.9 | [101] |
| Si substituting for Ti | | 1.625 | [101] |
| S-doped rutile $TiO_2$ | Photoreduction of water above 390 nm with sacrificial electron donor. | 2.34 | [120] |
| N-doped rutile $TiO_2$ | Photoreduction of water above 390 nm with sacrificial electron donor | 2.94 | [120] |
| C-doped rutile $TiO_2$, 1st onset | | **2.32** | [7] |
| C-doped rutile $TiO_2$, 2nd onset | | **2.82** (**1.83**) | [7] |
| Undoped | | 3.05 | a |
| B substituting for O | | 1.42 (**1.27**) | a |
| C substituting for O, 1st onset | | 2.36 (**1.57**) | a |
| C substituting for O, 2nd onset | | 2.73 | a |
| N substituting for O | | 2.5 | a |
| B interstitial, N substituting for O | | 2.62 | a |
| Ga substituting for O | | 0.5–0.9 | a |
| | *Anatase* | | |
| Undoped | No photodecomposition of acetaldehyde above 400 nm | 3.21 | [141] |
| 0.05Co/$TiO_2$ | Photodecomposition of acetaldehyde above 400 nm | 3.06 | [141] |
| 0.27Co/$TiO_2$ | | 3.06 | [141] |
| 1.8Co/$TiO_2$ (weak onset ca 775–800 nm) | | 3.06 | [141] |
| 2 wt% Pt substituting for Ti | | 2.74 | [142] |
| 1 wt% Pt substituting for Ti | | 2.77 | [142] |
| 0.5 wt% Pt substituting for Ti | | 2.77 | [142] |
| 0.2 wt% Pt substituting for Ti | Photodegradation of dichloroacetate under visible light | 2.86 | [142] |
| 0 wt% Pt substituting for Ti | No photodegradation of dichloroacetate under visible light | 2.91 | [142] |
| 0% Sb | No photodegradation of methylene blue | 2.84 | [127] |
| 1% Sb | 97.6% photodegradation of methylene blue | 2.08 | [127] |

Table 4: Continued.

| Composition | Activity notes | $E_g$ (eV) | Ref. |
|---|---|---|---|
| 5% Sb | 98.8% photodegradation of methylene blue | 1.91 | [127] |
| 1% Sb by organic solvent preparation | | 1.97 | [127] |
| $TiO_2$ | 5% photodegradation of methylene blue after 3 hours | 3.17 | [125] |
| N-doped and calcined at 400 C | 38% photodegradation of methylene blue after 3 hours | 2.26 | [125] |
| N-doped and calcined at 500 C | 35% photodegradation of methylene blue after 3 hours | 2.26 | [125] |
| N-doped and calcined at 600 C (some rutile) | 32% photodegradation of methylene blue after 3 hours | 2.31 | [125] |
| N-doped and calcined at 700 C (predominantly rutile) | 26% photodegradation of methylene blue after 3 hours | 2.91 | [125] |
| Prepared from Ti/thiourea mole ratio 1 : 0 | | 3.20 | [143] |
| Prepared from Ti/thiourea mole ratio 1 : 3 | Degradation of toulene under vis light relative to Degussa P25 [144] : ~12 | 2.67 | [143] |
| Prepared from Ti/thiourea mole ratio 1 : 2 | Degradation of toulene under vis light relative to Degussa P25 : ~15 | 2.88 | [143] |
| Prepared from Ti/thiourea mole ratio 1 : 1 | Degradation of toulene under vis light relative to Degussa P25 : ~10 | 3 | [143] |
| Prepared from Ti/thiourea mole ratio 1 : 0 | Degradation of toulene under vis light relative to Degussa P25 : ~1 | 3.19 | [143] |
| $TiO_2$ | | 3.2 | [145] |
| $TiO_2$ + 450°C treatment (anatase and rutile) | | 3.33 | [145] |
| $TiO_2$/Cr (amorphous) | | 2.2 | [145] |
| $TiO_2$/Cr + 450°C treatment (anatase and "a little rutile") | | 2.54 | [145] |
| $TiO_2$ (anatase with a little brookite) | Photocatalytic rate constant 0.003 | 3.22 | [122] |
| N-doped (anatase with a little brookite) | Photocatalytic rate constant 0.019 | 2.90 | [122] |
| N + Eu-doped (anatase with a little brookite) | Photocatalytic rate constant 0.025 | 2.85 | [122] |
| Hint of second onset in N + Eu-doped (anatase with a little brookite) | Photocatalytic rate constant 0.025 | 2.05 | [122] |
| Undoped | 80% pesticide remaining after 2.5 hours irradiation | 3.12 | [146] |
| 0.04% Mo substituting for Ti | 35% pesticide remaining after 2.5 hours irradiation | 2.81 | [146] |
| 0.06% Mo substituting for Ti | 25% pesticide remaining after 2.5 hours irradiation | 2.58 | [146] |
| 0.1% Mo substituting for Ti | 35% pesticide remaining after 2.5 hours irradiation | 2.75 | [146] |
| Undoped | 5% photodegradation of methylene blue after 2 hours | 3.45 | [121] |
| 5 at% N | 98% photodegradation of methylene blue after 2 hours | 2.75 | [121] |
| Undoped | Negligible decomposition of 4-chlorophenol under irradiation | 2.95 | [123] |
| N-doped | | 2.9 | [123] |

Table 4: Continued.

| Composition | Activity notes | $E_g$ (eV) | Ref. |
|---|---|---|---|
| I-doped | Decomposition of 4-chlorophenol under irradiation | 1.4–2.2 | [123] |
| Undoped | | 3.2 | [124] |
| 1.6 at% N | | 2.25 | [124] |
| 1.6 at% N second onset possibly from O vacancies. | | ~1.6 | [124] |
| Undoped | Negligible of photooxidation of acetone under irradiation | 3.00 | [147] |
| I-doped | Photooxidation of acetone under irradiation | 2.36 | [147] |
| Undoped | Photodegradation of malachite green rate 0.005 | 3.17 | [148] |
| Sn-doped | Photodegradation of malachite green rate 0.0175 | 2.55 | [148] |
| S-doped anatase $TiO_2$ | Photoreduction of water above 390 nm with sacrificial electron donor | 2.28 | [120] |
| N-doped anatase $TiO_2$ | Photoreduction of water above 390 nm with sacrificial electron donor | 2.58 | [120] |
| Degussa P25 | Relative degradation rate of acetaldehyde 0.213 | 3.16 | [128] |
| Degussa P25 hint of second onset, presumably from rutile component | Relative degradation rate of acetaldehyde 0.213 | 2.94 | [128] |
| Undoped | | 3.01 | [128] |
| C-doped | relative degradation rate of acetaldehyde 1.74 | 2.18 | [128] |
| $TiN_xO_yF_z$ calc. | | 1.8 | [99] |
| $TiN_xO_yF_z$ expt. | | 2.32 | [99] |
| $TiO_2$ calc.. | | 2.14 | [99] |
| $TiO_2$ expt. | | 3.26 | [99] |
| undoped | | 1.95 | [102] |
| N substitutional | | 1.83 | [102] |
| NH substitutional | | 1.83 | [102] |
| N interstitial | | 2.09 | [102] |
| NH interstitial | | 1.88 | [102] |
| N-doped by laser deposition in Nitrogen atmosphere | Degradation of methyl orange and methylene blue | 1.0 | [96] |
| N-doped by laser deposition in Nitrogen atmosphere | Degradation of methyl orange and methylene blue | 2.5 | [149] |

[(a)]present work.

an oxygen atom in the $TiO_2$ structure, the corresponding $2p$ orbitals "float" up in energy, into the band gap (see Figure 3). This places an impurity band in the gap. That this impurity band is slightly above the vbm and that the unpaired electron is nitrogen $2p$ in character is now quite well documented [113, 117]. The situation that is similar in rutile is similar to anatase, save for the fact that there is a simultaneous contraction of the valence band in rutile upon N-doping so that despite the presence of an impurity band just above the valance band edge, promotion of an electron from the impurity band to the cb is actually slightly blue-shifted relative to the undoped case.

Nitrogen doping is generally substitutional, replacing oxygen in the lattice to produce structures with the O–Ti–N XPS (X-ray photoelectron spectroscopy) signature [118]. There is some evidence [119] that the photoactive centers are actually V-NO-Ti, where V denotes a vacancy. XPS holds promise to reveal more detailed information about the nature of impurity sites in N-doped titania as some XPS peaks remain to be unambiguously assigned. Deeper insight into the nature of the impurity in N-doped titania comes from combined electron pair resonance (EPR) and DFT studies [113]. The N center within the bulk may be either neutral and paramagnetic, or anionic and diamagnetic. In the presence of oxygen vacancies the latter are favored. This can be understood in terms of the picture of the electronic structure in the presence of an oxygen vacancy presented above. The oxygen vacancy forces two electrons into the cb, localizing on neighboring Ti cations, reducing them to Ti(III). If a diamagnetic N center is present, the presence of the impurity state in the bg means that it is thermodynamically favorable for the N center to absorb

an electron from the cb, oxidizing the Ti back to Ti(IV). This has been elegantly demonstrated by the change in the EPR signal upon reduction of the material [113] and explains the lower oxygen vacancy formation energy in the presence of N impurities [117].

In contrast to the work of Diwald et al. [115], Nishijima and colleagues [120] found experimentally that nitrogen doping of rutile *decreases* the optical adsorption onset slightly from the undoped case (see Table 4) but produces a long tail of adsorption deep into the visible range (>500 nm). The apparent disagreement may arise from differences in the materials due to different preparation procedures. Nishijima and colleagues found a greater shift the in the onset for anatase, but again a long tail of adsorption to wavelengths >500 nm, as did Jagadale et al. [121]. Xu et al. found a similar onset for N-doped anatase [122], as did Tojo [123]. (These results are collected in Table 4.) One of the most dramatic shifts of the optical absorption onset into the visible range by nitrogen doping was reported in thin films prepared by atomic layer deposition [124]. Sathish et al. [125] studied N-doping of anatase as a function of calcination temperature. They found similar values for the absorption onset for anatase calcined at 400–600 C, but that calcination at 700 C resulted in predominantly rutile phase, with an onset comparable to pure rutile. They noted that this is at least in part due to a decrease in heteroatom doping with increasing calcination temperature. By interpretation of XPS spectra, Yamada et al. [12] showed that this decrease in vis-range adsorption and concomitant decrease in photocatalytic activity results from O atoms substituting for the N dopant atoms upon heating in air.

A theoretical study [126] of phosphorous doping of anatase found that substitution of P for O places P-3$p$ bands within the bg. It was predicted, however, that substitutional P-for-Ti doping (oxygen-rich conditions) is thermodynamically favored over substitutional P-for-O doping (Ti-rich conditions). Furthermore, optical transitions were reported to arise from vb $\rightarrow$ cb transition and did not involve the gap states.

Moon et al. [127] considered doping with Sb. Antimony is much more metallic in character than nitrogen or phosphorous. It was found that in addition to shifting the photoadsorption onset into the visible range, Sb doping arrests the anatase-to-rutile transition upon calcination. It also decreases the particle size and produces a corresponding increase in photocatalytic efficiency as measured by the decomposition of methyl bromide.

*4.2. Group IV-A Doping.* Yang et al. [128] have synthesized C-doped and C + V-codoped anatase. They found the greatest increase in photocatalytic activity with C-doping. This was likely partially due to the fact that C-doping produces the smallest particle size. Kang et al. [129] achieved C-doping by grinding anatase in the presence of ethanol with subsequent heat treatment. The grinding gradually converts the anatase to Srilankite and then to rutile. This process, which normally takes place at 600–700 C [71], can be partially arrested with urea [130]. Xu et al. [122] note that this is believed to result from N-doping leading to defects at grain boundaries, which in turn increase the barrier to atomic diffusion. The best visible-light photocatalytic activity was achieved after 2 hours of grinding. Further grinding reduces the activity.

As with nitrogen, in the atomic limit, the carbon 2$p$ orbitals are higher in energy than oxygen 2$p$ orbitals because their nuclear charges are smaller. When a carbon (or nitrogen) atom replaces an oxygen atom in the $TiO_2$ structure, the corresponding 2$p$ orbitals "float" up in energy, into the band gap (see Figure 3c). These bands appear clearly in the band structure for carbon-doped $TiO_2$ shown in Figure 4(c). Experimentally, evidence of states within the band gap arising from these levels for C-, N-, and S-doped titania has been found by XPS [118, 131]. This qualitative description makes clear the origin of the unusual "double onset" feature in the optical adsorption spectrum of carbon-doped $TiO_2$. Optical transitions between the carbon 2$p$ states within the band gap are forbidden to first order [57, 64] ($\Delta l = 0$). Transitions from these bands to the Ti 3$d$ bands within the conduction band are allowed. Sun et al. [65] confirm that new adsorption upon doping is not from band-to-band transition but from gap states to unoccupied stated in the cb [132]. In the case of C-doping, onset arises from excitation of an electron from the highest occupied carbon 2$p$ band to the cbm [92]. The second higher energy onset arises from excitation of an electron from the second-highest-energy occupied carbon 2$p$ band to the cbm. While lacking a distinct onset, the optical absorption spectrum of the closely related N-doped $TiO_2$ anatase shows measurable absorption below 500 nm (<2.4 eV) with hints of true onsets around 484 nm (2.6 eV) and 424 nm (2.9 eV) (see [6, Figure 2(b)]). This is again explained by the qualitative description of the band structure given in Figure 3. As with carbon, substituting nitrogen places N-2$p$ bands close above the vbm. These are visible in the band structure shown in Figure 4(b). Band structure diagrams, similar to Figure 4(b) here, can be found for N-doped [98], and N- and NH-doped anatase in [102]. The nitrogen 2$p$ states are clearly distinguishable above the vbm. Gombac and colleagues note that *interstitial* N-doping also produces both filled and occupied intergap states [13].

The computed results in Figure 4 are based on calculations with a $Ti_4O_7X$ supercell based on substitutional doping of $Ti_4O_8$. The dopant concentration is selected to produce a small unit cell with a stoichiometry close to that of the landmark experimental work of Kahn et al. [7] (our stoichiometry is $Ti_4O_7X$, that in the experimental work is $Ti_4O_{7.4}$,$C_{0.6}$.) To investigate the effect of changing the C-doping concentration, we enlarged the supercell to $3 \times 1 \times 1$ (2.5% C by mass), $2 \times 2 \times 1$ (1.9% C), and $2 \times 2 \times 2$ (0.94% C). In all cases the three C 2$p$-bands retain almost same position with respect to the $TiO_2$ band gap. This implies that heavy C-doping is not necessary to modify the optical properties of titania, a result that is consistent with experimental findings [133]. Increasing the C-doping concentration is evidently not an effective way to reduce the band gap. Experimental results show no direct relationship between dopant concentration and the optical adsorption edge in B-doped [134] and N-doped [98] titania

as well. In the case of N-doping, it has been argued [135] that high concentration of N might lead to TiN (which would be transparent) or many defects (which would serve as recombination centers). Clearly these outcomes would have undesirable implications for photocatalytic efficiency.

Calculations by Yang and colleagues [101] indicate that Si-doping of titania is quite different from C-doping. In the case of silicon doping, substitution of Si-for-Ti is energetically preferred over substitution of Si-for-O. The Si-3$p$ states are mostly within the vb and the small shift in the optical adsorption edge results from lowering the cbm.

*4.3. Group III-A Doping.* The observation that C-doping reduces the band gap by replacing oxygen 2$p$-orbitals in the valance band with C 2$p$-orbitals that float up into the band gap due to the weaker nuclear-electron interaction suggests that B-doping would further reduce the band gap because B has even weaker nuclear-electron interactions than C. This supposition is confirmed by the computed band structure for the $Ti_4O_7B$ supercell, shown in Figure 4(d). The basic features are the same as in the case of C-doping (Figure 4(c)) but just one electron occupies the highest occupied boron 2$p$-band. Similar placement of the boron 2$p$-bands was reported in the theoretical analysis of Jin and colleagues [136] who used a rutile (110) surface slab model. As shown in Table 4, the lowest transition energy in the case of B-doping is ca 1.42 eV, within in the visible region and ideal for efficient use of solar radiation [137]. In fact, In and colleagues report that B-doping of anatase results not only in appreciable adsorption in the visible range, but also in appreciable photocatalytic activity [56].

An experimental study of boron doping of anatase found "no linear relationship between the red shift and the boron content" and concluded that the B-doping must therefore be interstitial not substitutional [134]. While it is true that interstitial doping has been found to be energetically favored [136] (at least in the rutile case) the results for carbon-doping (discussed previosly) where we varied the C-doping concentration by enlarging the supercell suggest that the lack of correlation between the red-shift and dopant concentration does not necessarily confirm the presence of interstitial doping.

Detailed theoretical analysis of the energetics in the B-doping case has been presented by Jin et al. [136]. Using a rutile (110) surface slab model, they report generally lower values for the formation energy than our estimate reported in Table 3. They find B-doping into interstitial sites to be favored over substitutional doping, and that the doping of subsurface interstitial sites is thermodynamically spontaneous in a Ti-rich environment. The cell volume expansion upon B-doping is apparently slightly larger in the case of anatase [36].

Two theoretical studies have considered cation doping by Al, that is, $Al^{3+}$ substituting for $Ti^{4+}$. Stevenson and colleagues [138] found that substitutional doping by Al is favored over interstitial doping, and that such doping facilitates the rutile $\rightarrow$ anatase transition. Islam et al. [139] showed that $Al^{3+}$ substituting for $Ti^{4+}$ introduces a defect state with the unpaired spin localized on an oxygen neighbor. They further showed that the defect state is removed by introduction of a charge-compensating substitution of O by Cl.

In Ga, the nuclear-electron interactions are even weaker than in B. This suggests that a smaller band gap may be achieved with Ga-for-O substitutional doping. First-principles calculations support this hypothesis. The predicted transition energies are 0.5 and 0.9 eV. Furthermore, the calculated formation energy for Ga-doping (Table 3) is even smaller than for C-doping, which has been produced successfully by different groups, suggesting that Ga-doped rutile is a high value synthetic target.

*4.4. Doping by Higher Chalcogens.* Since $TiO_2$ is an oxide, oxygen-doping is not practical, but there has been interest in doping with sulfur. Randeniya and colleagues [150] have shown that S-doping can be achieved in multiple ways, such as ball milling with S, ball milling with thiourea, and sol-gel with tetrabutyl titanate and thiourea. S-doping has been shown to be very similar to P-doping in terms of influence on the electronic structure [126]. As with P-doping, S-for-Ti substitution is preferred over S-for-O substitution. In general, low dopant concentrations reduce the photoadsorption energy by mixing S-3$p$ states with O-2$p$ states from the vb [151]. This is a case where the dopant concentration does appear to have a significant effect on the optical transitions. Higher concentrations broaden the band and further reduce the band gap. This increase in visible-range adsorption is accompanied by an increase in photocatalytic decomposition of methylene blue upon irradiation with visible light [140]. There is experimental evidence to confirm that $S^{6+}$-for-$Ti^{4+}$ substitution is energetically favored over $S^{2-}$ for-$O^{2-}$ substitution [140, 143].

*4.5. Halogen Doping.* Any F-doping should not reduce the band gap since the F 2$p$-bands are far below the vbm as shown in Figure 4(e). This is borne out by several experimental investigations that show essentially no change in the optical adsorption edge upon F-doping [152–155]. As shown in Table 4, F-doping also has no appreciable effect on the crystal structure, a result that is also consistent with some experiments [154], but it has been proposed that enhancements in photocatalytic activity of titania upon F-doping are due to improved crystallinity of the material [156]. Li et al. [157] give compelling evidence that some component of the enhanced catalytic activity of F-doped titania arises from the generation of new surface acid sites. By comparing temperature-programmed desorption experiments with $NH_3$ on N-doped, F-doped, NF-doped, and undoped titania, they found a broad ammonia desorption peak only in the presence of F-doping [67].

Despite the fact that the optical and structural properties remain relatively unchanged, F-doping does yield enhanced photocatalytic activity. This may result from localization of the unpaired electron onto a single Ti atom [153]. A similar enhancement in catalytic activity was seen for F-doped $TiO_2$ nanotubes [158]. The Ti(III) that arises from F-doping may

serve to reduce the recombination rate of electrons and holes, thereby increasing the time that they are available to carry out catalysts [159, 160].

F-doping of $TiO_2$ yields a large energy benefit. The addition of an F atom adds three atomic $2p$-orbitals at about 6.6 eV below the vbm, but only five electrons. One valence band electron may therefore "fall" into the lone half-filled F $2p$-orbital, gaining as much as 6 eV. This hypothesis is supported by first-principles calculations. Note low formation energies of the F-doped materials in Table 3. We have further tested this hypothesis with calculations of $Ti_4O_7BF$. B is doped substitutionally and F is doped interstitially. This selection was based on the simple size argument that F, being smaller than B, should be placed in the more confined interstitial position. (The reverse, with B interstitial and F substitutional is also plausible.) The formation energy is indeed much lower than for B-doping alone. There is a tradeoff between reducing the band gap and lowering the formation energy. The one electron from the half-filled B $2p$-band moves to the lone half-filled F $2p$-band. The band gap is then larger because the highest energy B $p$-electron drops into the half-filled F $p$-band, so the optical transition takes place from the lowest B $p$-band, not the second lowest B $p$-band as in the B-doped case. (See Figure 3, which shows that the BF-doped case is like B-doped case except the transition is from lowest $p$-state, not from middle $p$-state.) Experimental studies [161] indeed show an "absorption edge around 535 nm, signifying that creation of the interband gap states produces an effective band gap of 2.4 eV." The gap states arise from the B $2p$ as the F $2p$ lie deep in the vb.

A further possible complication in B + F codoping is the formation of compounds of B and F. In the presence of excess fluorine and oxygen, the decomposition of $Ti_4O_7BF$ by the reaction,

$$Ti_4O_7BF + F_{2(g)} + \frac{1}{2}O_{2(g)} \longrightarrow Ti_4O_8 + BF_{3(g)}, \tag{7}$$

is energetically favored by 14.8 eV per formula unit. This reaction may be disfavored by carrying out the doping in under very low $O_2$ partial pressure, but the thermodynamic driving force for the production of $BF_3$ is so large that it may force the titania to go nonstoichiometric to produce the needed oxygen. A rough demonstration of this is as follows: Using the data in Table 3 we may write.

$$Ti_4O_7B + \frac{1}{2}O_{2(g)} \longrightarrow Ti_4O_8 + \frac{1}{m}B_{m(s)} \quad \Delta E = -8.3\,\text{eV}, \tag{8a}$$

$$Ti_4O_7BF + F_{2(g)} + \frac{1}{2}O_{2(g)} \longrightarrow Ti_4O_8 + BF_{3(g)} \quad \Delta E = -14.8\,\text{eV}, \tag{8b}$$

$$Ti_4O_8 + \frac{1}{2}F_{2(g)} + \frac{1}{m}B_{m(s)} \longrightarrow Ti_4O_7BF + \frac{1}{2}O_{2(g)} \quad \Delta E = 3.5\,\text{eV}. \tag{8c}$$

In addition, the oxygen vacancy formation energy in titania has been reported to be 4.2 eV [14], so we may write

$$Ti_4O_8 \longrightarrow Ti_4O_7 + \frac{1}{2}O_{2(g)} \quad \Delta E = 4.2\,\text{eV}. \tag{9}$$

Summing reactions (8a) through (9) yields

$$Ti_4O_7B + \frac{3}{2}F_{2(g)} \longrightarrow Ti_4O_7 + BF_{3(g)} \quad \Delta E = -15.4\,\text{eV}, \tag{10}$$

demonstrating that attempting to dope $Ti_4O_7B$ with fluorine will lead to nonstoichiometric titania and boron triflouride. Indeed, it has been suggested that some of the band gap narrowing in B + F codoped titania arises from oxygen vacancies [161], which are known to introduce defect states into the band gap [11, 108].

The production of $BF_{3(g)}$ upon attempt to dope $Ti_4O_7F$ with boron is endothermic. The reactions,

$$Ti_4O_7F + \frac{1}{2}O_{2(g)} \longrightarrow Ti_4O_8 + \frac{1}{2}F_{2(g)} \quad \Delta E = -0.18\,\text{eV}, \tag{11a}$$

$$\frac{1}{3}Ti_4O_7BF + \frac{1}{3}F_{2(g)} + \frac{1}{6}O_{2(g)} \longrightarrow \frac{1}{3}Ti_4O_8 + \frac{1}{3}BF_{3(g)} \quad \Delta E = \frac{1}{3}(-14.8)\,\text{eV}, \tag{11b}$$

$$\frac{1}{3}Ti_4O_8 + \frac{1}{6}F_{2(g)} + \frac{1}{3m}B_{m(s)} \longrightarrow \frac{1}{3}Ti_4O_7BF + \frac{1}{6}O_{2(g)} \quad \Delta E = \frac{1}{3}(3.5)\,\text{eV}, \tag{11c}$$

combined with reaction (9) yield

$$Ti_4O_7F + \frac{1}{3m}B_{m(s)} \longrightarrow Ti_4O_7 + \frac{1}{3}BF_{3(g)} \quad \Delta E = 0.25\,\text{eV}, \tag{12}$$

which suggests that latter approach may be a more fruitful avenue to B + F codoping.

In contrast to F-doping, which has no appreciable effect on the optical adsorption edge, I-doping results in a very significant decrease in the band gap (see Table 4). Tojo et al. [123] found optical transitions in the 1.4–2.2 eV range. They were able to determine that I-doping results in $I^{+5}$ substituting for $TI^{+4}$. This is a totally different doping mode than the case of F-doping, where F atoms are interstitial or substituting for oxygen as discussed above. A study of I-doping by Su et al. [147] reported adsorption in the 400–550 nm range and found that the most prominent impurity band arises from bridging I atoms on the surface.

A systematic theoretical analysis of halogen doping of titania is reported in [100]. For X substituting for Ti, there is a progression of the X-$np$ band from within the vb in case

of F, to within the bg in case of Cl and Br, to within the cb in case of I, whereupon the I-5s band actually lifts into bg. This progression is analogous to the case shown in Figure 3(c), where $2p$ bands due to a second-row nonmetal dopant are shifted relative to those of oxygen based on the change in nuclear charge. The theoretical analysis [100] further shows that I as a dopant exists is $I^{+5}$, Br as $Br^{4+}$, Cl as $Cl^{4+}$, and F as $F^{3+}$. Consequently, I is in an octahedral environment, but the others are Jahn-Teller distorted.

*4.6. Multiple Dopants.* Recently there has been increasing interest in modifying $TiO_2$ by introducing multiple dopants. One possible motivation for doing so is to combine the beneficial influences of two or more dopants. In an example discussed previously [157], N + F co-doping produces a material with a reduced band gap (due to N impurity bands withing the bg) and also surface acid sites, (due to the presence of F). As also discussed previosly, co-doping with F can also lower the formation energy. A second motivation for using multiple dopants is to offset the undesirable impacts of a dopant that introduces both desirable and undesirable features. In an example detailed below [162], co-doping with Cr + Sb, the Sb provides the extra electron needed to reduce $Cr^{+4}$ to its preferred $Cr^{3+}$ oxidation state without the necessity of forming a compensating oxygen vacancy.

A few other cases of multiple doping not discussed elsewhere in this paper merit note the following. Several dopants can be simultaneously incorporated by employing a molecular precursor. For example using thiourea and titinate nanotubes, Dong and colleagues were able to accomplish N + C + S co-doping [143]. It was found that S substitutes for Ti, C predominantly substitutes for Ti, and N is interstitial and substitutes for O. The optical bg proved quite sensitive to the thiourea : titinate mole ratio.

Li et al. [163] achieved B + N co-doping with titanium tetra-n-butyl oxide plus boric acid and urea. They report that, "The results indicate that the effect of boron doping on visible-light absorption is minor, and the absorption of B–N–$TiO_2$ comes mainly from nitrogen doping [163]." Combined theoretical and experimental studies show that B + N co-doping has superior catalytic activity to either N or B-doping alone, and that it is sensitive to concentration [13]. Interstitial N-doping creates both filled and unoccupied intragap states. Transitions to cb give rise to vis adsorptions. Interstitial B-doping creates 5-fold coordinated $Ti^{+3}$ at the surface, which can generate reactive superoxide species.

Chen and Burda [131] note that, "compared to pure $TiO_2$, additional absorptions up to 800 nm were observed for the C-, S-, and N-doped nanomaterials. The improved absorption can be divided into roughly two parts: 415–550 nm (shoulder) and 550 ~ 800 nm (tail) for N-doped $TiO_2$, 390–490 nm (shoulder) and 490 ~ 800 nm (tail) for C-doped $TiO_2$, and 390 ~ 800 nm (tail) for S-doped $TiO_2$. Among the three, the modification of the optical properties is the largest for N-doped $TiO_2$, although its dopant concentration is the lowest."

*4.7. TM Doping.* Zhanpeisov and Anpo [164] used simple cluster models of rutile and anatase and investigated changes in the HOMO-LUMO gap upon substitution of a single $Ti^{4+}$ by another transition metal TM cation. They found that, "the order of changes in the (LUMO-HOMO) energy difference is $Ni^{4+}$ < $Co^{4+}$ < $Cr^{4+}$ < $Mn^{4+}$ < $Fe^{4+}$ < $V^{4+}$ < $Ti^{4+}$." A study of Co-doped and Co-Fe co-doped anatase found a small decrease in the band gap that is independent of Co concentration [141]. The experiments did not unambiguously distinguish the position of the dopant atoms. At the highest concentrations there is a weak onset ca 775–800 nm (see Table 4). By contrast, Kim et al. [142] found band gap narrowing in direct proportion to the level of Pt-doping in anatase. A study of Cr-doped anatase found a significant decrease in the photoadsorption onset (see Table 4), which was partially retained upon annealing even after partial conversion of the anatase to rutile [145]. Another study of Cr-doping [165] was able to assign the transition at 450 nm as $Cr^{3+} \rightarrow Ti^{4+}$ or $^4A_{2g} \rightarrow {}^4T_{1g}$ of $Cr^3$, and the transition at 800 nm as $^4A_{2g} \rightarrow {}^4T_{2g}$ d–d transitions of $Cr^{3+}$. A comprehensive kinetic phase diagram for Fe doping has been presented by Zhang et al. [166].

A detailed theoretical study of TM doping used 48-atom supercells with 2 Ti substituted by $3d$ TM atoms, corresponds to 12.5 wt% [167]. It was found that as the atomic number of the dopant increases, the potential at dopant site becomes deeper and states shift down, first into bg then below the vbm. It was also noted that adjacent dopants lower the formation energy more than uniformly distributed dopants, but the "physics is similar." This downward shift of the dopant bands with increasing nuclear charge is analogous to the case shown in Figure 3(c) where the $2p$ bands shift up when carbon is substituted for oxygen because of the decrease in nuclear charge.

A study of Mo-doping by Devi and Murthy [146] found a nonmonatonic variation in the band gap with Mo concentration. The lattice parameter $c$, however, was found to expand linearly with dopant concentration. Doping was reported to take the form of $Mo^{6+}$ substituting for $Ti^{4+}$ with compensating O vacancies. It was reported that, "The optical absorption in the wavelength range 400–550 nm results from sub-band transitions closely related to the ionized oxygen vacancies and also due to the transitions from the mid band gaps formed by the Mo-doping." A study of Mo-doping of $TiO_2$ films found the remarkable result that doping of the bottom of the film produced a much greater enhancement in photocatalytic activity than doping the surface or uniformly [168]. It was speculated that bottom doping produces a barrier to electron-hole recombination.

To modify the optical and photocatalytic properties of $TiO_2$, doping with nonmetals has generally been more successful than doping with metal atoms [117]. This may be not only, at least in part, because the introduction of metal cations often requires specailzed equipment [157], but also because metal doping can result in increased charge carrier trapping [118]. Very recently, however, Di Valentin et al. [162] demonstrated a very cleverly designed co-doping with Cr and Sb. Observing that the presence of an oxygen vacancy leaves behind cb electrons than can more easily reduce $Cr^{4+}$

to its preferred $Cr^{3+}$ oxidation state than $Ti^{4+}$ to $Ti^{3+}$, they noted that introducing a Sb substitutional for Ti can furnish the extra electron to reduce $Cr^{4+}$ to its preferred $Cr^{3+}$ without the need for a compensating oxygen vacancy.

A study of Zr + S co-doping found doping does not produce a distinct onset of adsorption in vis range, but does enhance the broad tail in vis range [15]. The catalytic activity (as measured by photocatalytic degradation of toluene) followed the trend, $Zr–TiO_2–S > TiO_2–S > Zr–TiO_2 > TiO_2$, which was interpreted as a particle size effect. A study of V + C co-doping by Yang and colleagues [128] found that $V^{5+}$ substitutes for Ti and introduces an electron that can be excited to the cb with thermal energy. This forms a superoxide radical that degrades acetlyaldehyde in the dark, that is, a nonphotocatalytic reaction. Ta + N co-doping [68] shows weak but broad photoadsorption shoulders extending well into vis region for various Ta and N concentration ratios. The authors argue that vis photocatalytic activity from anion doping is weak compared to UV because vis light sensitivity arises from a narrow dopant *p* band with low reducing power and probably also low hole mobility. A theoretical study [108] of N + Nd co-doping with N substituting for O and Nd for Ti found N states just above the vbm and also defect states, likely form O vacancies, near the cb.

Doping with inner transitions elements (rare earths (Re)) produces small red shifts with the effect of doping at the 0.5 wt% level following the trend: $Gd^{3+} > Nd^{3+} > La^{3+} > Pr^{3+}$ ($Er^{3+}$) $> Ce^{3+} > Sm^{3+}$ [169]. It was proposed that this shift is due to charge transfer of rare earth f-electrons into the $TiO_2$ cb. There is some indication of the formation of Re oxides on the surface. More details of Eu doping can be found in [122]. The presence of the spectroscopic signature of the Eu-O-Ti species suggests Eu substitutes for Ti. Eu co-doping with nitrogen produces a hint of a second photoadsorption onset at longer wavelengvths (see Table 4).

*4.8. Alternative Theoretical Approaches.* Virtually all theoretical investigations of doped titania have employed supercell structural models using periodic boundary conditions and some implementation of density functional theory. These approximations are suitable because the materials are typically crystalline and investigation of optical properties requires use of methods that yield an explicit description of the electronic structure. Empirical potential-based methods have been employed in cases where an explicit description of the electronic structure is not required, such as the MD work of Naicker et al. [76] (in which the surface energy of titania nanoparticles was investigated) and the atomistic simulations of high pressure phases reported by Swamy et al. [72]. There are, however, a few notable exceptions to these typical choices of methodology. As noted above, Zhanpeisov and Anpo [164] used small cluster models to represent bulk titania and investigated the effect of substituting a single TM atom on the HOMO-LUMO gap, as an estimate of the effect of TM doping on the band gap in the bulk material. Steveson et al. [138] used much larger clusters ($Ti_{56}O_{112}$ for anatase and $Ti_{90}O_{180}$ for rutile) with pseudoatoms to terminate dangling bonds to investigate Al doping. They were able to show that Al doping favors the rutile → anatase transition.

## 5. Conclusions

In conclusion, there is intense interest in modifying the optical and photocatalytic properties of titania. Herein we have presented an overview of $TiO_2$ phases and reviewed results of recent studies of doped $TiO_2$. Doping studies have already sampled a significant fraction of the periodic table and the results often follow logical periodic trends. This should afford better targeting of future doping efforts.

A reasonable qualitative understanding of the influence of dopant atoms on the electronic structure is afforded by recognizing that, in general, in $TiO_2$ the valance band is oxygen-2*p* in character and the conduction band is titanium 3*d* & 4*s* in character. One can roughly place the defect states introduced by a dopant atom by considering the placement of its valance orbitals relative to oxygen-2*p* and titanium 3*d* & 4*s*. This interpretation holds up under first-principles calculations and can be used to explain the displacement of the Fermi level with the introduction of vacancies, and the presence of multiple onsets in the photoadsorption spectrum of doped materials. In addition to introducing defect states, many dopants appear to alter the band gap by introducing oxygen vacancies, which places defect states near the conduction band.

Based on the results reviewed here it is predicted that Ga-doping of rutile has an energy cost comparable to species that have been previously synthesized, and that Ga-doped rutile may produce a very small band gap. This suggests that Ga-doped titania is a high-value synthetic target.

While the crystalline lattice parameters of the phases of titania are assessable to calculation, accurate theoretical predictions of the band gap and related spectroscopic onsets remain elusive. A few nontraditional theoretical approaches to calculate the band gap in crystalline materials promise more accurate estimation of the band gap than traditional LDA. These merit further investigation and it is hoped that this paper will stimulate further studies.

## Acknowledgments

K. Sohlberg acknowledges the support of catalytic materials research by the USDoE under Contract no. DE-FC02-01CH11085 and by NSF-GOALI Grant no. DMR-0111841. Some of the computations were supported by NCSA under Grant CHE990015N.

## References

[1] A. Fujishima and K. Honda, "Electrochemical photolysis of water at a semiconductor electrode," *Nature*, vol. 238, no. 5358, pp. 37–38, 1972.

[2] A. L. Linsebigler, G. Lu, and J. T. Yates Jr., "Photocatalysis on $TiO_2$ surfaces: principles, mechanisms, and selected results," *Chemical Reviews*, vol. 95, no. 3, pp. 735–758, 1995.

[3] A. Hameed, M. A. Gondal, and Z. H. Yamani, "Effect of transition metal doping on photocatalytic activity of $WO_3$ for

water splitting under laser illumination: role of 3d-orbitals," *Catalysis Communications*, vol. 5, no. 11, pp. 715–719, 2004.

[4] P. J. D. Lindan, N. M. Harrison, J. M. Holender, and M. J. Gillan, "First-principles molecular dynamics simulation of water dissociation on $TiO_2$ (110)," *Chemical Physics Letters*, vol. 261, no. 3, pp. 246–252, 1996.

[5] M. S. Reisch, "Rainbow in a can," *Chemical and Engineering News*, vol. 81, no. 44, pp. 25–28, 2003.

[6] R. Asahi, T. Morikawa, T. Ohwaki, K. Aoki, and Y. Taga, "Visible-light photocatalysis in nitrogen-doped titanium oxides," *Science*, vol. 293, no. 5528, pp. 269–271, 2001.

[7] S. U. M. Khan, M. Al-Shahry, and W. B. Ingler Jr., "Efficient photochemical water splitting by a chemically modified n-$TiO_2$," *Science*, vol. 297, no. 5590, pp. 2243–2245, 2002.

[8] R. Schaub, P. Thostrup, N. Lopez, et al., "Oxygen vacancies as active sites for water dissociation on rutile $TiO_2$ (110)," *Physical Review Letters*, vol. 87, no. 26, Article ID 266104, 4 pages, 2001.

[9] M. Li, W. Hebenstreit, L. Gross, et al., "Oxygen-induced restructuring of the $TiO_2$ (110) surface: a comprehensive study," *Surface Science*, vol. 437, no. 1, pp. 173–190, 1999.

[10] M. Ramamoorthy, R. D. King-Smith, and D. Vanderbilt, "Defects on $TiO_2$ (110) surfaces," *Physical Review B*, vol. 49, no. 11, pp. 7709–7715, 1994.

[11] N. Serpone, "Is the band gap of pristine $TiO_2$ narrowed by anion- and cation-doping of titanium dioxide in second-generation photocatalysts?" *Journal of Physical Chemistry B*, vol. 110, no. 48, pp. 24287–24293, 2006.

[12] K. Yamada, H. Yamane, S. Matsushima, et al., "Effect of thermal treatment on photocatalytic activity of N-doped $TiO_2$ particles under visible light," *Thin Solid Films*, vol. 516, no. 21, pp. 7482–7487, 2008.

[13] V. Gombac, L. De Rogatis, A. Gasparotto, et al., "$TiO_2$ nanopowders doped with boron and nitrogen for photocatalytic applications," *Chemical Physics*, vol. 339, no. 1–3, pp. 111–123, 2007.

[14] C. Di Valentin, G. Pacchioni, and A. Selloni, "Theory of carbon doping of titanium dioxide," *Chemistry of Materials*, vol. 17, no. 26, pp. 6656–6665, 2005.

[15] S. W. Kim, R. Khan, T.-J. Kim, and W.-J. Kim, "Synthesis, characterization, and application of Zr,S co-doped $TiO_2$ as visible-light active photocatalyst," *Bulletin of the Korean Chemical Society*, vol. 29, no. 6, pp. 1217–1223, 2008.

[16] M. S. A. Abdel-Mottaleb, V. Augugliaro, and L. Palmisano, Eds., "Doped $TiO_2$ nanomaterials and applications," *International Journal of Photoenergy*, vol. 2008, Article ID 419096, 2008.

[17] C. Di Valentin, U. Diebold, and A. Selloni, Eds., "Doping and functionalization of photoactive semiconducting metal oxides," *Chemical Physics*, vol. 339, no. 1–3, 2007.

[18] J. P. Perdew, K. Burke, and M. Ernzerhof, "Generalized gradient approximation made simple," *Physical Review Letters*, vol. 77, no. 18, pp. 3865–3868, 1996.

[19] C. Lee, W. Yang, and R. G. Parr, "Development of the Colle-Salvetti correlation-energy formula into a functional of the electron density," *Physical Review B*, vol. 37, no. 2, pp. 785–789, 1988.

[20] A. D. Becke, "Density-functional exchange-energy approximation with correct asymptotic behavior," *Physical Review A*, vol. 38, no. 6, pp. 3098–3100, 1988.

[21] P. J. Stephens, F. J. Devlin, C. F. Chabalowski, and M. J. Frisch, "Ab Initio calculation of vibrational absorption and circular dichroism spectra using density functional force fields," *Journal of Physical Chemistry*, vol. 98, no. 45, pp. 11623–11627, 1994.

[22] A. D. Becke, "Density-functional thermochemistry. III. The role of exact exchange," *The Journal of Chemical Physics*, vol. 98, no. 7, pp. 5648–5652, 1993.

[23] M. Lazzeri, A. Vittadini, and A. Selloni, "Structure and energetics of stoichiometric $TiO_2$ anatase surfaces," *Physical Review B*, vol. 63, no. 15, Article ID 155409, 9 pages, 2001.

[24] J. K. Burdett, T. Hughbanks, G. J. Miller, J. W. Richardson Jr., and J. V. Smith, "Structural-electronic relationships in inorganic solids: powder neutron diffraction studies of the rutile and anatase polymorphs of titanium dioxide at 15 and 295 K," *Journal of the American Chemical Society*, vol. 109, no. 12, pp. 3639–3646, 1987.

[25] D. T. Chomer and K. Herrington, "The structures of anatase and rutile," *Journal of the American Chemical Society*, vol. 77, no. 18, pp. 4708–4709, 1955.

[26] S.-D. Mo and W. Y. Ching, "Electronic and optical properties of three phases of titanium dioxide: rutile, anatase, and brookite," *Physical Review B*, vol. 51, no. 19, pp. 13023–13032, 1995.

[27] H. Peng, "First-principles study of native defects in rutile $TiO_2$," *Physics Letters A*, vol. 372, no. 9, pp. 1527–1530, 2008.

[28] J. Muscat, N. M. Harrison, and G. Thornton, "Effects of exchange, correlation, and numerical approximations on the computed properties of the rutile $TiO_2$ (100) surface," *Physical Review B*, vol. 59, no. 3, pp. 2320–2326, 1999.

[29] P. J. D. Lindan, N. M. Harrison, M. J. Gillan, and J. A. White, "First-principles spin-polarized calculations on the reduced and reconstructed $TiO_2$ (110) surface," *Physical Review B*, vol. 55, no. 23, pp. 15919–15927, 1997.

[30] K. M. Glassford and J. R. Chelikowsky, "Structural and electronic properties of titanium dioxide," *Physical Review B*, vol. 46, no. 3, pp. 1284–1298, 1992.

[31] P. Jelinek, H. Wang, J. P. Lewis, O. F. Sankey, and J. Ortega, "Multicenter approach to the exchange-correlation interactions in ab initio tight-binding methods," *Physical Review B*, vol. 71, no. 23, Article ID 235101, 9 pages, 2005.

[32] A. Beltran, L. Gracia, and J. Andres, "Density functional theory study of the brookite surfaces and phase transitions between natural titania polymorphs," *Journal of Physical Chemistry B*, vol. 110, no. 46, pp. 23417–23423, 2006.

[33] R. Asahi, Y. Taga, W. Mannstadt, and A. J. Freeman, "Electronic and optical properties of anatase $TiO_2$," *Physical Review B*, vol. 61, no. 11, pp. 7459–7465, 2000.

[34] J. S. Olsen, L. Gerward, and J. Z. Jiang, "On the rutile/[alpha]-$PbO_2$-type phase boundary of $TiO_2$," *Journal of Physics and Chemistry of Solids*, vol. 60, no. 2, pp. 229–233, 1999.

[35] J. Pascual, J. Camassel, and H. Mathieu, "Fine structure in the intrinsic absorption edge of $TiO_2$," *Physical Review B*, vol. 18, no. 10, pp. 5606–5614, 1978.

[36] K. Y. Dai and B. Huang, "Origin of the photoactivity in boron-doped anatase and rutile $TiO_2$ calculated from first principles," *Physical Review B*, vol. 76, Article ID 195201, 2007.

[37] H. Zhang and J. F. Banfield, "Thermodynamic analysis of phase stability of nanocrystalline titania," *Journal of Materials Chemistry*, vol. 8, no. 9, pp. 2073–2076, 1998.

[38] T. Arlt, M. Bermejo, M. A. Blanco, et al., "High-pressure polymorphs of anatase $TiO_2$," *Physical Review B*, vol. 61, no. 21, pp. 14414–14419, 2000.

[39] M. Koelsch, S. Cassaignon, J. F. Guillemoles, and J. P. Jolivet, "Comparison of optical and electrochemical properties of anatase and brookite $TiO_2$ synthesized by the sol-gel method," *Thin Solid Films*, vol. 403-404, pp. 312–319, 2002.

[40] W. H. Baur, "Atomabstände und Bindungswinkel im Brookit, $TiO_2$," *Acta Crystallographica*, vol. 14, part 3, pp. 214–216, 1961.

[41] W. Luo, S. F. Yang, Z. C. Wang, et al., "Structural phase transitions in brookite-type $TiO_2$ under high pressure," *Solid State Communications*, vol. 133, no. 1, pp. 49–53, 2005.

[42] D. Reyes-Coronado, G. Rodríguez-Gattorno, M.E. Espinosa-Pesqueira, C. Cab, R. de Coss, and G. Oskam, "Phase-pure $TiO_2$ nanoparticles: anatase, brookite and rutile," *Nanotechnology*, vol. 19, no. 14, Article ID 145605, 2008.

[43] R. Buonsanti, V. Grillo, E. Carlino, et al., "Nonhydrolytic synthesis of high-quality anisotropically shaped brookite $TiO_2$ nanocrystals," *Journal of the American Chemical Society*, vol. 130, no. 33, pp. 11223–11233, 2008.

[44] A. E. Morales, E. Sanchez Mora, and U. Pal, "Use of diffuse reflectance spectroscopy for optical characterization of unsupported nanostructures," *Revista Mexicana de Fisica S*, vol. 53, no. 5, pp. 18–22, 2007.

[45] W. Kohn and L. J. Sham, "Self-consistent equations including exchange and correlation effects," *Physical Review*, vol. 140, no. 4, pp. A1133–A1138, 1965.

[46] M. S. Hybertsen and S. G. Louie, "First-principles theory of quasiparticles: calculation of band gaps in semiconductors and insulators," *Physical Review Letters*, vol. 55, no. 13, pp. 1418–1421, 1985.

[47] Y. Zhang, W. Lin, Y. Li, K. Ding, and J.-Q. Li, "A theoretical study on the electronic structures of $TiO_2$: effect of Hartree-Fock exchange," *Journal of Physical Chemistry B*, vol. 109, no. 41, pp. 19270–19277, 2005.

[48] J. Muscat, A. Wander, and N. M. Harrison, "On the prediction of band gaps from hybrid functional theory," *Chemical Physics Letters*, vol. 342, no. 3-4, pp. 397–401, 2001.

[49] D. Muñoz, N. M. Harrison, and F. Illas, "Electronic and magnetic structure of $LaMnO_3$ from hybrid periodic density-functional theory," *Physical Review B*, vol. 69, no. 8, Article ID 085115, 9 pages, 2004.

[50] X.-B. Feng and N. M. Harrison, "Electronic structure of $CaCuO_2$ from the B3LYP hybrid density functional," *Physical Review B*, vol. 69, no. 13, Article ID 132502, 2004.

[51] J. P. Perdew and W. Yue, "Accurate and simple density functional for the electronic exchange energy: generalized gradient approximation," *Physical Review B*, vol. 33, no. 12, pp. 8800–8802, 1986.

[52] J. P. Perdew, "Density-functional approximation for the correlation energy of the inhomogeneous electron gas," *Physical Review B*, vol. 33, no. 12, pp. 8822–8824, 1986.

[53] D. C. Langreth and M. J. Mehl, "Beyond the local-density approximation in calculations of ground-state electronic properties," *Physical Review B*, vol. 28, no. 4, pp. 1809–1834, 1983.

[54] D. C. Langreth and J. P. Perdew, "Theory of nonuniform electronic systems. I. Analysis of the gradient approximation and a generalization that works," *Physical Review B*, vol. 21, no. 12, pp. 5469–5493, 1980.

[55] H. Wang and J. P. Lewis, "Effects of dopant states on photoactivity in carbon-doped $TiO_2$," *Journal of Physics: Condensed Matter*, vol. 17, no. 21, pp. L209–L213, 2005.

[56] S. In, A. Orlov, R. Berg, et al., "Effective visible light-activated B-doped and B,N-codoped $TiO_2$ photocatalysts," *Journal of the American Chemical Society*, vol. 129, no. 45, pp. 13790–13791, 2007.

[57] X. Nie, S.-H. Wei, and S. B. Zhang, "Bipolar doping and band-gap anomalies in delafossite transparent conductive oxides," *Physical Review Letters*, vol. 88, no. 6, Article ID 066405, 4 pages, 2002.

[58] A. C. Withers, E. J. Essene, and Y. Zhang, "Rutile/$TiO_2$II phase equilibria," *Contributions to Mineralogy and Petrology*, vol. 145, no. 2, pp. 199–204, 2003.

[59] H. Kato, K. Asakura, and A. Kudo, "Highly efficient water splitting into $H_2$ and $O_2$ over lanthanum-doped $NaTaO_3$ photocatalysts with high crystallinity and surface nanostructure," *Journal of the American Chemical Society*, vol. 125, no. 10, pp. 3082–3089, 2003.

[60] S. Wang, A. Y. Borisevich, S. N. Rashkeev, et al., "Dopants adsorbed as single atoms prevent degradation of catalysts," *Nature Materials*, vol. 3, no. 3, pp. 143–146, 2004.

[61] A. Testino, I. R. Bellobono, V. Buscaglia, et al., "Optimizing the photocatalytic properties of hydrothermal $TiO_2$ by the control of phase composition and particle morphology. A systematic approach," *Journal of the American Chemical Society*, vol. 129, no. 12, pp. 3564–3575, 2007.

[62] M. Anpo, T. Shima, S. Kodama, and Y. Kubokawa, "Photocatalytic hydrogenation of $CH_3CCH$ with $H_2O$ on small-particle $TiO_2$: size quantization effects and reaction intermediates," *Journal of Physical Chemistry*, vol. 91, no. 16, pp. 4305–4310, 1987.

[63] M. Valden, X. Lai, and D. W. Goodman, "Onset of catalytic activity of gold clusters on titania with the appearance of nonmetallic properties," *Science*, vol. 281, no. 5383, pp. 1647–1650, 1998.

[64] X. Nie, S.-H. Wei, and S. B. Zhang, "First-principles study of transparent p-type conductive $SrCu_2O_2$ and related compounds," *Physical Review B*, vol. 65, no. 7, Article ID 075111, 8 pages, 2002.

[65] H. Sun, Y. Bai, W. Jin, and N. Xu, "Visible-light-driven $TiO_2$ catalysts doped with low-concentration nitrogen species," *Solar Energy Materials and Solar Cells*, vol. 92, no. 1, pp. 76–83, 2008.

[66] R. Scotti, I. R. Bellobono, C. Canevali, et al., "Sol-gel pure and mixed-phase titanium dioxide for photocatalytic purposes: relations between phase composition, catalytic activity, and charge-trapped sites," *Chemistry of Materials*, vol. 20, no. 12, pp. 4051–4061, 2008.

[67] D. Li, N. Ohashi, S. Hishita, T. Kolodiazhnyi, and H. Haneda, "Origin of visible-light-driven photocatalysis: a comparative study on N/F-doped and N-F-codoped $TiO_2$ powders by means of experimental characterizations and theoretical calculations," *Journal of Solid State Chemistry*, vol. 178, no. 11, pp. 3293–3302, 2005.

[68] K. Obata, H. Irie, and K. Hashimoto, "Enhanced photocatalytic activities of Ta, N co-doped $TiO_2$ thin films under visible light," *Chemical Physics*, vol. 339, no. 1–3, pp. 124–132, 2007.

[69] R. Nakamura, A. Okamoto, H. Osawa, H. Irie, and K. Hashimoto, "Design of all-inorganic molecular-based photocatalysts sensitive to visible light: Ti(IV)-O-Ce(III) bimetallic assemblies on mesoporous silica," *Journal of the American Chemical Society*, vol. 129, no. 31, pp. 9596–9597, 2007.

[70] H. Irie, S. Miura, K. Kamiya, and K. Hashimoto, "Efficient visible light-sensitive photocatalysts: Grafting Cu(II) ions onto $TiO_2$ and $WO_3$ photocatalysts," *Chemical Physics Letters*, vol. 457, no. 1–3, pp. 202–205, 2008.

[71] R. Ren, Z. Yang, and L. L. Shaw, "Polymorphic transformation and powder characteristics of $TiO_2$ during high energy milling," *Journal of Materials Science*, vol. 35, no. 23, pp. 6015–6026, 2000.

[72] V. Swamy, J. D. Gale, and L. S. Dubrovinsky, "Atomistic simulation of the crystal structures and bulk moduli of $TiO_2$ polymorphs," *Journal of Physics and Chemistry of Solids*, vol. 62, no. 5, pp. 887–895, 2001.

[73] P. Waldner and G. Eriksson, "Thermodynamic modelling of the system titanium-oxygen," *Calphad*, vol. 23, no. 2, pp. 189–218, 1999.

[74] K. Sohlberg, "Introducing the core concepts of nano-science and nanotechnology: two vignettes," *Journal of Chemical Education*, vol. 83, p. 1516, 2006.

[75] G. P. Pez, A. R. Scott, A. C. Cooper, and H. Cheng, "Hydrogen storage by reversible hydrogenation of pi-conjugated substrates," US patent no. 7351395.

[76] P. K. Naicker, P. T. Cummings, H. Zhang, and J. F. Banfield, "Characterization of titanium dioxide nanoparticles using molecular dynamics simulations," *Journal of Physical Chemistry B*, vol. 109, no. 32, pp. 15243–15249, 2005.

[77] S. T. Aruna, S. Tirosh, and A. Zaban, "Nanosize rutile titania particle synthesis via a hydrothermal method without mineralizers," *Journal of Materials Chemistry*, vol. 10, no. 10, pp. 2388–2391, 2000.

[78] W. Wang, B. Gu, L. Liang, W. A. Hamilton, and D. J. Wesolowski, "Synthesis of rutile (alpha-$TiO_2$) nanocrystals with controlled size and shape by low-temperature hydrolysis: effects of solvent composition," *Journal of Physical Chemistry B*, vol. 108, no. 39, pp. 14789–14792, 2004.

[79] A. Zaban, S. T. Aruna, S. Tirosh, B. A. Gregg, and Y. Mastai, "The effect of the preparation condition of $TiO_2$ colloids on their surface structures," *Journal of Physical Chemistry B*, vol. 104, no. 17, pp. 4130–4133, 2000.

[80] G. Oskam and F. D. P. Poot, "Synthesis of ZnO and $TiO_2$ nanoparticles," *Journal of Sol-Gel Science and Technology*, vol. 37, no. 3, pp. 157–160, 2006.

[81] H. Kominami, Y. Ishii, M. Kohno, S. Konishi, Y. Kera, and B. Ohtani, "Nanocrystalline brookite-type titanium(IV) oxide photocatalysts prepared by a solvothermal method: correlation between their physical properties and photocatalytic activities," *Catalysis Letters*, vol. 91, no. 1-2, pp. 41–47, 2003.

[82] B. I. Lee, X. Wang, R. Bhave, and M. Hu, "Synthesis of brookite $TiO_2$ nanoparticles by ambient condition sol process," *Materials Letters*, vol. 60, no. 9-10, pp. 1179–1183, 2006.

[83] M. Ramamoorthy, D. Vanderbilt, and R. D. King-Smith, "First-principles calculations of the energetics of stoichiometric $TiO_2$ surfaces," *Physical Review B*, vol. 49, no. 23, pp. 16721–16727, 1994.

[84] D. Vanderbilt, "Soft self-consistent pseudopotentials in a generalized eigenvalue formalism," *Physical Review B*, vol. 41, no. 11, pp. 7892–7895, 1990.

[85] M. C. Payne, M. P. Teter, D. C. Allan, T. A. Arias, and J. D. Joannopoulos, "Iterative minimization techniques for ab initio total-energy calculations: molecular dynamics and conjugate gradients," *Reviews of Modern Physics*, vol. 64, no. 4, pp. 1045–1097, 1992.

[86] *DACAPO pseudopotential code*, 2003, .dtu.dk/software.aspx http://www.camd.

[87] J. P. Perdew and Y. Wang, "Accurate and simple analytic representation of the electron-gas correlation energy," *Physical Review B*, vol. 45, no. 23, pp. 13244–13249, 1992.

[88] G. Charlten, P. B. Howes, C. L. Nicklin, et al., "Relaxation of $TiO_2$ (110)-$(1 \times 1)$ using surface X-ray diffraction," *Physical Review Letters*, vol. 78, no. 3, pp. 495–498, 1997.

[89] J. Muscat and N. M. Harrison, "The physical and electronic structure of the rutile (001) surface," *Surface Science*, vol. 446, no. 1-2, pp. 119–127, 2000.

[90] P. Vinet, J. Ferrante, J. R. Smith, and J. H. Rose, "A universal equation of state for solids," *Journal of Physics C*, vol. 19, pp. L467–L473, 1986.

[91] C. Wolverton and K. C. Hass, "Phase stability and structure of spinel-based transition aluminas," *Physical Review B*, vol. 63, no. 2, Article ID 024102, 6 pages, 2001.

[92] X. Nie and K. Sohlberg, "The influence of surface reconstruction and C-impurities on photocatalytic water dissociation by $TiO_2$," *Materials Research Society Symposium Proceedings*, vol. 801, pp. 205–210, 2003, paper no. BB6.6.1.

[93] B. J. Morgan and G. W. Watson, "A density functional theory + $U$ study of oxygen vacancy formation at the (110), (100), (101), and (001) surfaces of rutile $TiO_2$," *Journal of Physical Chemistry C*, vol. 113, no. 17, pp. 7322–7328, 2009.

[94] F. Labat, P. Baranek, and C. Adamo, "Structural and electronic properties of selected rutile and anatase $TiO_2$ surfaces: an ab initio investigation," *Journal of Chemical Theory and Computation*, vol. 4, no. 2, pp. 341–352, 2008.

[95] Z. Hua, D. Songyuan, and W. Kongjia, "First-principles investigation of (001) surface of $TiO_2$," *Plasma Science & Technology*, vol. 6, pp. 2467–2474, 2004.

[96] X. Q. Gong and A. Selloni, "First-principles study of the structures and energetics of stoichiometric brookite $TiO_2$ surfaces," *Physical Review B*, vol. 76, Article ID 235307, 2007.

[97] F. Aryasetiawan and O. Gunnarsson, "The GW method," *Reports on Progress in Physics*, vol. 61, no. 3, pp. 237–312, 1998.

[98] K. Yang, Y. Dai, and B. Huang, "Study of the nitrogen concentration influence on N-doped $TiO_2$ anatase from first-principles calculations," *Journal of Physical Chemistry C*, vol. 111, no. 32, pp. 12086–12090, 2007.

[99] K. Maeda, Y. Shimodaira, B. Lee, et al., "Studies on $TiN_xO_yF_z$ as a visible-light-responsive photocatalyst," *Journal of Physical Chemistry C*, vol. 111, no. 49, pp. 18264–18270, 2007.

[100] K. Yang, Y. Dai, B. Huang, and M.-H. Whangbo, "Density functional characterization of the band edges, the band gap states, and the preferred doping sites of halogen-doped $TiO_2$," *Chemistry of Materials*, vol. 20, no. 20, pp. 6528–6534, 2008.

[101] K. Yang, Y. Dai, and B. Huang, "First-principles calculations for geometrical structures and electronic properties of Si-doped $TiO_2$," *Chemical Physics Letters*, vol. 456, no. 1–3, pp. 71–75, 2008.

[102] L. Mi, Y. Zhang, and P.-N. Wang, "First-principles study of the hydrogen doping influence on the geometric and electronic structures of N-doped $TiO_2$," *Chemical Physics Letters*, vol. 458, no. 4–6, pp. 341–345, 2008.

[103] R. V. Kasowski and R. H. Tait, "Theoretical electronic properties of $TiO_2$ (rutile) (001) and (110) surfaces," *Physical Review B*, vol. 20, no. 12, pp. 5168–5177, 1979.

[104] P. I. Sorantin and K. Schwarz, "Chemical bonding in rutile-type compounds," *Inorganic Chemistry*, vol. 31, no. 4, pp. 567–576, 1992.

[105] V. E. Henrich, G. Dresselhaus, and H. J. Zeiger, "Observation of two-dimensional phases associated with defect states on the surface of $TiO_2$," *Physical Review Letters*, vol. 36, no. 22, pp. 1335–1339, 1976.

[106] S.-G. Wang, X.-D. Wen, D.-B. Cao, Y.-W. Li, J. Wang, and H. Jiao, "Formation of oxygen vacancies on the $TiO_2(110)$ surfaces," *Surface Science*, vol. 577, no. 1, pp. 69–76, 2005.

[107] Y. Lu, M. Hirohashi, and K. Sato, "Thermoelectric properties of non-stoichiometric titanium dioxide $TiO_{2-x}$ fabricated by reduction treatment using carbon powder," *Materials Transactions*, vol. 47, no. 6, pp. 1449–1452, 2006.

[108] Y. Wang and D. J. Doren, "First-principles calculations on $TiO_2$ doped by N, Nd, and vacancy," *Solid State Communications*, vol. 136, no. 3, pp. 186–189, 2005.

[109] R. Schaub, E. Wahlstrom, A. Ronnau, E. Lagsgaard, I. Stensgaard, and F. Besenbacher, "Oxygen-mediated diffusion of oxygen vacancies on the $TiO_2$ (110) surface," *Science*, vol. 299, no. 5605, pp. 377–379, 2003.

[110] X. Cui, B. Wang, Z. Wang, et al., "Formation and diffusion of oxygen-vacancy pairs on $TiO_2$ (110)-$(1 \times 1)$," *Journal of Chemical Physics*, vol. 129, no. 4, Article ID 044703, 2008.

[111] C. Di Valentin, G. Pacchioni, and A. Selloni, "Electronic structure of defect states in hydroxylated and reduced rutile $TiO_2$ (110) surfaces," *Physical Review Letters*, vol. 97, no. 16, Article ID 166803, 2006.

[112] V. E. Henrich and R. L. Kurtz, "Surface electronic structure of $TiO_2$: atomic geometry, ligand coordination, and the effect of adsorbed hydrogen," *Physical Review B*, vol. 23, no. 12, pp. 6280–6287, 1981.

[113] S. Livraghi, M. C. Paganini, E. Giamello, A. Selloni, C. Di Valentin, and G. Pacchioni, "Origin of photoactivity of nitrogen-doped titanium dioxide under visible light," *Journal of the American Chemical Society*, vol. 128, no. 49, pp. 15666–15671, 2006.

[114] H. Irie, Y. Watanabe, and K. Hashimoto, "Nitrogen-concentration dependence on photocatalytic activity of $TiO_{2-x}N_x$ powders," *Journal of Physical Chemistry B*, vol. 107, no. 23, pp. 5483–5486, 2003.

[115] O. Diwald, T. L. Thompson, E. G. Goralski, S. D. Walck, and J. T. Yates Jr., "The effect of nitrogen ion implantation on the photoactivity of $TiO_2$ rutile single crystals," *Journal of Physical Chemistry B*, vol. 108, no. 1, pp. 52–57, 2004.

[116] C. Di Valentin, G. Pacchioni, A. Selloni, S. Livraghi, and E. Giamello, "Characterization of paramagnetic species in N-doped $TiO_2$ powders by EPR spectroscopy and DFT calculations," *Journal of Physical Chemistry B*, vol. 109, no. 23, pp. 11414–11419, 2005.

[117] C. Di Valentin, G. Pacchioni, and A. Selloni, "Origin of the different photoactivity of N-doped anatase and rutile $TiO_2$," *Physical Review B*, vol. 70, no. 8, Article ID 085116, 2004.

[118] X. Chen and C. Burda, "Photoelectron spectroscopic investigation of nitrogen-doped titania nanoparticles," *Journal of Physical Chemistry B*, vol. 108, no. 40, pp. 15446–15449, 2004.

[119] C. Feng, Y. Wang, Z. Jin, et al., "Photoactive centers responsible for visible-light photoactivity of N-doped $TiO_2$," *New Journal of Chemistry*, vol. 32, no. 6, pp. 1038–1047, 2008.

[120] K. Nishijima, T. Kamai, N. Murakami, T. Tsubota, and T. Ohno, "Photocatalytic hydrogen or oxygen evolution from water over S- or N-doped $TiO_2$ under visible light," *International Journal of Photoenergy*, vol. 2008, Article ID 173943, 7 pages, 2008.

[121] T. C. Jagadale, S. P. Takale, R. S. Sonawane, et al., "N-doped $TiO_2$ nanoparticle based visible light photocatalyst by modified peroxide sol-gel method," *Journal of Physical Chemistry C*, vol. 112, no. 37, pp. 14595–14602, 2008.

[122] J. Xu, Y. Ao, D. Fu, and C. Yuan, "A simple route for the preparation of Eu, N-codoped $TiO_2$ nanoparticles with enhanced visible light-induced photocatalytic activity," *Journal of Colloid and Interface Science*, vol. 328, no. 2, pp. 447–451, 2008.

[123] S. Tojo, T. Tachikawa, M. Fujitsuka, and T. Majima, "Iodine-doped $TiO_2$ photocatalysts: correlation between band structure and mechanism," *Journal of Physical Chemistry C*, vol. 112, no. 38, pp. 14948–14954, 2008.

[124] H.-E. Cheng, W.-J. Lee, C.-M. Hsu, M.-H. Hon, and C.-L. Huang, "Visible light activity of nitrogen-doped $TiO_2$ thin films grown by atomic layer deposition," *Electrochemical and Solid-State Letters*, vol. 11, pp. D81–D84, 2008.

[125] M. Sathish, B. Viswanathan, and R. P. Viswanath, "Characterization and photocatalytic activity of N-doped $TiO_2$ prepared by thermal decomposition of Ti-melamine complex," *Applied Catalysis B*, vol. 74, no. 3-4, pp. 307–312, 2007.

[126] K. Yang, Y. Dai, and B. Huang, "Understanding photocatalytic activity of S- And P-doped $TiO_2$ under visible light from first-principles," *Journal of Physical Chemistry C*, vol. 111, no. 51, pp. 18985–18994, 2007.

[127] J. Moon, H. Takagi, Y. Fujishiro, and M. Awano, "Preparation and characterization of the Sb-doped $TiO_2$ photocatalysts," *Journal of Materials Science*, vol. 36, no. 4, pp. 949–955, 2001.

[128] X. Yang, C. Cao, K. Hohn, et al., "Highly visible-light active C- and V-doped $TiO_2$ for degradation of acetaldehyde," *Journal of Catalysis*, vol. 252, no. 2, pp. 296–302, 2007.

[129] I.-C. Kang, Q. Zhang, S. Yin, T. Sato, and F. Saito, "Preparation of a visible sensitive carbon doped $TiO_2$ photo-catalyst by grinding $TiO_2$ with ethanol and heating treatment," *Applied Catalysis B*, vol. 80, no. 1-2, pp. 81–87, 2008.

[130] S. C. Pillai, P. Periyat, R. George, et al., "Synthesis of high-temperature stable anatase $TiO_2$ photocatalyst," *Journal of Physical Chemistry C*, vol. 111, no. 4, pp. 1605–1611, 2007.

[131] X. Chen and C. Burda, "The electronic origin of the visible-light absorption properties of C-, N- and S-doped $TiO_2$ nanomaterials," *Journal of the American Chemical Society*, vol. 130, no. 15, pp. 5018–5019, 2008.

[132] T. Lindgren, J. M. Mwabora, E. Avendano, et al., "Photoelectrochemical and optical properties of nitrogen doped titanium dioxide films prepared by reactive DC magnetron sputtering," *Journal of Physical Chemistry B*, vol. 107, no. 24, pp. 5709–5716, 2003.

[133] S. Sakthivel and H. Kisch, "Daylight photocatalysis by carbon-modified titanium dioxide," *Angewandte Chemie International Edition*, vol. 42, no. 40, pp. 4908–4911, 2003.

[134] R. Khan, S. W. Kim, T.-J. Kim, and C.-M. Nam, "Comparative study of the photocatalytic performance of boron-iron Co-doped and boron-doped $TiO_2$ nanoparticles," *Materials Chemistry and Physics*, vol. 112, no. 1, pp. 167–172, 2008.

[135] Z. Lin, A. Orlov, R. M. Lambert, and M. C. Payne, "New insights into the origin of visible light photocatalytic activity of nitrogen-doped and oxygen-deficient anatase $TiO_2$," *Journal of Physical Chemistry B*, vol. 109, no. 44, pp. 20948–20952, 2005.

[136] H. Jin, Y. Dai, W. Wei, and B. Huang, "Density functional characterization of B doping at rutile $TiO_2$ (110) surface," *Journal of Physics D*, vol. 41, no. 19, Article ID 195411, 2008.

[137] O. Khaselev and J. A. Turner, "A monolithic photovoltaic-photoelectrochemical device for hydrogen production via water splitting," *Science*, vol. 280, no. 5362, pp. 425–427, 1998.

[138] M. Steveson, T. Bredow, and A. R. Gerson, "MSINDO quantum chemical modelling study of the structure of aluminium-doped anatase and rutile titanium dioxide," *Physical Chemistry Chemical Physics*, vol. 4, no. 2, pp. 358–365, 2002.

[139] M. M. Islam, T. Bredow, and A. Gerson, "Electronic properties of oxygen-deficient and aluminum-doped rutile $TiO_2$ from first principles," *Physical Review B*, vol. 76, Article ID 045217, 2007.

[140] T. Ohno, M. Akiyoshi, T. Umebayashi, K. Asai, T. Mitsui, and M. Matsumura, "Preparation of S-doped $TiO_2$ photocatalysts and their photocatalytic activities under visible light," *Applied Catalysis A*, vol. 265, no. 1, pp. 115–121, 2004.

[141] M. Iwasaki, M. Hara, H. Kawada, H. Tada, and S. Ito, "Cobalt ion-doped $TiO_2$ photocatalyst response to visible light," *Journal of Colloid and Interface Science*, vol. 224, no. 1, pp. 202–204, 2000.

[142] S. Kim, S.-J. Hwang, and W. Choi, "Visible light active platinum-ion-doped $TiO_2$ photocatalyst," *Journal of Physical Chemistry B*, vol. 109, no. 51, pp. 24260–24267, 2005.

[143] F. Dong, W. Zhao, and Z. Wu, "Characterization and photocatalytic activities of C, N and S co-doped $TiO_2$ with 1D nanostructure prepared by the nano-confinement effect," *Nanotechnology*, vol. 19, no. 36, Article ID 365607, 2008.

[144] T. Ohno, K. Sarukawa, K. Tokieda, and M. Matsumura, "Morphology of a $TiO_2$ photocatalyst (Degussa, P-25) consisting of anatase and rutile crystalline phases," *Journal of Catalysis*, vol. 203, no. 1, pp. 82–86, 2001.

[145] W.-Y. Ho, M.-H. Chan, K.-S. Yao, C.-L. Chang, D.-Y. Wang, and C.-H. Hsu, "Characteristics of chromium-doped titanium oxide coatings synthesized by cathodic arc deposition," *Thin Solid Films*, vol. 516, no. 23, pp. 8530–8536, 2008.

[146] L. G. Devi and B. N. Murthy, "Characterization of Mo doped $TiO_2$ and its enhanced photo catalytic activity under visible light," *Catalysis Letters*, vol. 125, no. 3-4, pp. 320–330, 2008.

[147] W. Su, Y. Zhang, Z. Li, et al., "Multivalency iodine doped $TiO_2$: preparation, characterization, theoretical studies, and visible-light photocatalysis," *Langmuir*, vol. 24, no. 7, pp. 3422–3428, 2008.

[148] F. Sayilkan, M. Asilturk, P. Tatar, et al., "Photocatalytic performance of Sn-doped $TiO_2$ nanostructured thin films for photocatalytic degradation of malachite green dye under UV and VIS-lights," *Materials Research Bulletin*, vol. 43, no. 1, pp. 127–134, 2008.

[149] L. Zhao, Q. Jiang, and J. Lian, "Visible-light photocatalytic activity of nitrogen-doped $TiO_2$ thin film prepared by pulsed laser deposition," *Applied Surface Science*, vol. 254, no. 15, pp. 4620–4625, 2008.

[150] L. K. Randeniya, A. B. Murphy, and I. C. Plumb, "A study of S-doped $TiO_2$ for photoelectrochemical hydrogen generation from water," *Journal of Materials Science*, vol. 43, no. 4, pp. 1389–1399, 2008.

[151] T. Umebayashi, T. Yamaki, H. Itoh, and K. Asai, "Band gap narrowing of titanium dioxide by sulfur doping," *Applied Physics Letters*, vol. 81, no. 3, pp. 454–456, 2002.

[152] N. Todorova, T. Giannakopoulou, G. Romanos, T. Vaimakis, J. Yu, and C. Trapalis, "Preparation of fluorine-doped $TiO_2$ photocatalysts with controlled crystalline structure," *International Journal of Photoenergy*, vol. 2008, Article ID 534038, 9 pages, 2008.

[153] A. M. Czoska, S. Livraghi, M. Chiesa, et al., "The nature of defects in fluorine-doped $TiO_2$," *Journal of Physical Chemistry C*, vol. 112, no. 24, pp. 8951–8956, 2008.

[154] T. Giannakopoulou, N. Todorova, T. Vaimakis, S. Ladas, and C. Trapalis, "Study of fluorine-doped $TiO_2$ sol-gel thin coatings," *Journal of Solar Energy Engineering*, vol. 130, no. 4, Article ID 041007, 5 pages, 2008.

[155] J. Xu, Y. Ao, D. Fu, and C. Yuan, "Synthesis of fluorine-doped titania-coated activated carbon under low temperature with high photocatalytic activity under visible light," *Journal of Physics and Chemistry of Solids*, vol. 69, no. 10, pp. 2366–2370, 2008.

[156] A. Hattori, K. Shimoda, H. Tada, and S. Ito, "Photoreactivity of sol-gel $TiO_2$ films formed on soda-lime glass substrates: effect of SiO2 underlayer containing fluorine," *Langmuir*, vol. 15, no. 16, pp. 5422–5425, 1999.

[157] D. Li, H. Haneda, S. Hishita, and N. Ohashi, "Visible-light-driven N-F-codoped $TiO_2$ photocatalysts. 1. Synthesis by spray pyrolysis and surface characterization," *Chemistry of Materials*, vol. 17, no. 10, pp. 2588–2595, 2005.

[158] Y. Yu, H.-H. Wu, B.-L. Zhu, et al., "Preparation, characterization and photocatalytic activities of F-doped $TiO_2$ nanotubes," *Catalysis Letters*, vol. 121, no. 1-2, pp. 165–171, 2008.

[159] J. Yu, X. Zhao, and Q. Zhao, "Photocatalytic activity of nanometer $TiO_2$ thin films prepared by the sol-gel method," *Materials Chemistry and Physics*, vol. 69, pp. 25–29, 2001.

[160] J. C. Yu, J. Yu, W. Ho, Z. Jiang, and L. Zhang, "Effects of F-doping on the photocatalytic activity and microstructures of nanocrystalline $TiO_2$ powders," *Chemistry of Materials*, vol. 14, no. 9, pp. 3808–3816, 2002.

[161] E. A. Reyes-Garcia, Y. Sun, and D. Raftery, "Solid-state characterization of the nuclear and electronic environments in a boron-fluoride co-doped $TiO_2$ visible-light photocatalyst," *Journal of Physical Chemistry C*, vol. 111, no. 45, pp. 17146–17154, 2007.

[162] C. D. Valentin, G. Pacchioni, H. Onishi, and A. Kudo, "Cr/Sb co-doped $TiO_2$ from first principles calculations," *Chemical Physics Letters*, vol. 469, no. 1–3, pp. 166–171, 2009.

[163] Y. Li, G. Ma, S. Peng, G. Lu, and S. Li, "Boron and nitrogen co-doped titania with enhanced visible-light photocatalytic activity for hydrogen evolution," *Applied Surface Science*, vol. 254, no. 21, pp. 6831–6836, 2008.

[164] N. U. Zhanpeisov and M. Anpo, "Theoretical ab initio study of the intrinsic band gap in semiconductor oxides based on modified titanium dioxides," *Theoretical Chemistry Accounts*, vol. 114, no. 1–3, pp. 235–241, 2005.

[165] X. Fan, X. Chen, S. Zhu, et al., "The structural, physical and photocatalytic properties of the mesoporous Cr-doped $TiO_2$," *Journal of Molecular Catalysis A*, vol. 284, no. 1-2, pp. 155–160, 2008.

[166] Y. Zhang, S. G. Ebbinghaus, A. Weidenkaff, et al., "Controlled iron-doping of macrotextures nanocrystalline titania," *Chemistry of Materials*, vol. 15, pp. 4028–4033, 2003.

[167] H. Peng, J. Li, S.-S. Li, and J.-B. Xia, "First-principles study of the electronic structures and magnetic properties of 3d transition metal-doped anatase $TiO_2$," *Journal of Physics: Condensed Matter*, vol. 20, no. 12, Article ID 125207, 2008.

[168] Y. Yang, X. Li, J. Chen, and L. Wang, "Effect of doping mode on the photocatalytic activities of Mo/$TiO_2$," *Journal of Photochemistry and Photobiology A*, vol. 163, no. 3, pp. 517–522, 2004.

[169] A.-W. Xu, Y. Gao, and H.-Q. Liu, "The preparation, characterization, and their photocatalytic activities of rare-earth-doped $TiO_2$ nanoparticles," *Journal of Catalysis*, vol. 207, no. 2, pp. 151–157, 2002.